Click Here for Full Article

Geochemical character of serpentinites associated with high- to ultrahigh-pressure metamorphic rocks in the Alps, Cuba, and the Himalayas: Recycling of elements in subduction zones

Kéiko H. Hattori

Department of Earth Sciences, University of Ottawa, 140 Louis Pasteur, Ottawa, Ontario, Canada K1N 6N5 (khattori@uottawa.ca)

Stéphane Guillot

LGCA, University of Grenoble, UMR5025, OSUG, UJF, 1381 Rue de la Piscine, BP 53, F–38041 Grenoble Cedex 9, France (sguillot@ujf–grenoble.fr)

[1] Serpentinites associated with eclogitic rocks were examined from three areas: the Alps, Cuba, and the Himalayas. Most serpentinites have low Al/Si and high concentrations of Ir-type platinum group elements (PGE) in bulk rock compositions, indicating that they are hydrated mantle peridotites. A few samples contain high Al/Si and low concentrations of Ir-type PGE, suggesting that they are ultramafic cumulates. Among the hydrated mantle peridotites, we identified two groups, primarily on the basis of Al/Si and Mg/Si ratios: forearc mantle serpentinites and hydrated abyssal peridotites. Forearc serpentinites occur in the Himalayas and along a major deformation zone in Cuba. All serpentinites in the Alps and most serpentinites in Cuba are hydrated abyssal peridotites. Himalayan serpentinites have low Al/Si and high Mg/Si ratios in bulk rock compositions, and high Cr in spinel; they were serpentinized by fluids released from the subducted Indian continent and enriched in fluid-mobile elements, and show high $^{87}Sr/^{86}Sr$, up to 0.730, similar to the values of rocks of the subducted margin of the Indian continent. Although Himalayan serpentinites have a similar refractory geochemical signature as the Mariana forearc serpentinites, the former contain markedly high concentrations of fluid-mobile elements and high $^{87}Sr/^{86}Sr$ compared to the latter that were hydrated by subducted Pacific Ocean crust. The data indicate that the enrichment of fluid-mobile elements in forearc serpentinites depends on the composition of subducted slabs. Alpine serpentinites and most Cuban serpentinites show moderate Al/Si similar to abyssal peridotites. Hydration of peridotites near the seafloor is supported by micro-Raman spectra of earlier formed lizardite, high $\delta^{34}S$ (+11 to +17‰) of sulphides, and elevated $^{87}Sr/^{86}Sr$, ranging from 0.7037 to 0.7095. The data support the contribution of S and Sr from seawater and sediments. These serpentinites are not highly enriched in fluid-mobile elements because serpentinization occurred at a high water/rock ratio. Alkali elements are conspicuously unenriched in all serpentinites. This lack of alkali enrichment is explained by slab retention of alkalis. This is also consistent with the observation of relatively low alkali concentrations in volcanic front magmas, since partial melting related to the volcanic fronts is triggered by dehydration of serpentinites.

1. Introduction

[2] Serpentinites are important in subduction zones because they contain up to 13 wt% water, and are stable at considerable depths, down to ∼100 km [e.g., *Wünder et al.*, 2001]. Thus serpentinites are large reservoirs of water and effective vehicles for its transport from the shallow crust to the mantle. Water is essential for the production of arc magmas and in the transfer of elements from slabs to mantle wedges and from mantle wedges to arc magmas. In addition, because of their physical properties, serpentinites may contribute to a variety of processes in subduction zones. For example, buoyant serpentinites, compared to anhydrous peridotites, may play a significant role in the exhumation of ultrahigh pressure (UHP) and high pressure (HP) metamorphic rocks [e.g., *Schwartz et al.*, 2001], and the large volume change associated with the dehydration of serpentinites may be responsible for deep seismic activity in subduction zones [e.g., *Dobson et al.*, 2002].

[3] Our earlier studies of serpentinites associated with the Tso Morari UHP unit in the Himalayas demonstrated that these serpentinites originated from the base of the mantle wedge underlying Eurasia, with the precursor peridotites hydrated by waters released from the margin of the Indian continent [e.g., *Guillot et al.*, 2001; *Hattori and Guillot*, 2003]. Our interpretation is consistent with the growing geophysical evidence, including seismic, electrical and magnetic data, for the occurrence of hydrated forearc-mantle peridotites in many subduction zones [e.g., *Kamiya and Kobayashi*, 2000; *Bostock et al.*, 2002; *Brocher et al.*, 2003; *Blakely et al.*, 2005; *Soyer and Unworth*, 2006].

[4] In oceanic subduction zones, voluminous serpentinites are closely associated with omphacitic eclogitic rocks that were originally oceanic basalts and gabbros [e.g., *Pognante and Kienast*, 1987; *Hacker*, 1996]. The common occurrence of serpentinites on the Atlantic ocean floor [e.g., *Cannat*, 1993; *Cannat et al.*, 1997] and other slow- to ultraslow-spreading oceanic lithosphere [e.g., *Horen et al.*, 1996; *Dick et al.*, 2003; *Mével*, 2003; *Bach et al.*, 2002] suggest that some of these serpentinites may have originated from oceanic lithosphere [e.g., *Lagabrielle and Cannat*, 1990; *Scambelluri et al.*, 1997].

[5] This paper presents chemical, mineralogical and isotope data for serpentinites associated with HP and UHP rocks in three orogenic belts: the Himalayas, the Alps and Cuba. In the Himalayas, HP and UHP rocks have a metasedimentary origin, and were deposited on the margin of the Indian continent. In the latter two locations, UHP and HP rocks originated from subducted oceanic basalts and gabbros [e.g., *Pognante and Kienast*, 1987; *Schneider et al.*, 2004]. Petrogenetic studies of many igneous rocks commonly use large-ion lithophile elements to infer their origins. However, serpentinites contain low concentrations of such elements. In addition, many large-ion lithophile elements are highly mobile during serpentinization. Therefore we use compatible and fluid-immobile elements to characterize the protoliths of these serpentinites.

2. Samples

2.1. Himalayas

[6] We examined serpentinites in the Tertiary subduction complex of the Ladakh area, northwest Himalayas. The subduction complex formed during the closure of the Tethyan ocean by subduction of oceanic crust, by accretion of the Nidar and
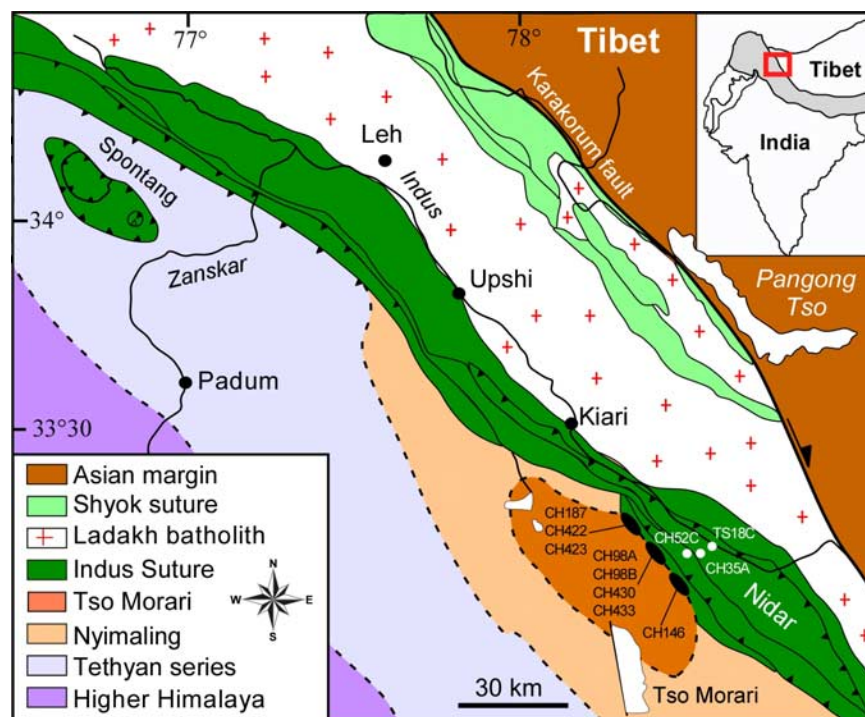
Figure 1a. Geological map of Ladakh area in northwestern India showing sample locations along the northern edge of the Tso Morari massif and in the Indus suture zone. Solid circles are villages and towns. Map modified after *Guillot et al.* [2001]. Samples CH35A and TS18C were collected at the base of the highly deformed Nidar arc complex (labeled "Nidar" in the Indus Suture zone of the map). CH52C came from the Drakkarpo unit, which is an accreted oceanic island just south of the Nidar ophiolite complex. Both are in the Indus Suture Zone.

Spontang oceanic arcs, and by the eventual subduction of the margin of the Indian continent beneath Eurasia [e.g., *Guillot et al.*, 2001]. Samples (CH98A, CH 98B, CH146, CH187, CH422, CH423, CH430, CH433) were collected from discontinuous lenses of serpentinites, 100 × 1000 m in size, along the Zildat fault in contact with the Tso Morari UHP unit, 100 × 50 km in size (Figure 1a). The Tso Morari unit was once a shallow-water sedimentary sequence deposited on the margin of the Indian continent prior to being subducted beneath Eurasia at ~55 Ma [*Guillot et al.*, 2001; *Leech et al.*, 2005]. The sedimentary rocks reached a depth of ~100 km and a temperature of ~600 °C at ~50 Ma [*O'Brien et al.*, 2001; *de Sigoyer et al.*, 2004] before being exhumed together with the serpentinites. For comparison, we also used serpentinite samples from the Indus Suture Zone (Figure 1a). Samples CH35A and TS18C were collected at the base of the highly deformed Nidar arc ophiolite complex and CH52C from the tectonic mélange of the Drakkarpo unit, which is an accreted oceanic island [*Guillot et al.*, 2000] (Figure 1a).

2.2. Alps

[7] The western Alps formed during subduction of the Piedmont-Liguria domain of the Tethyan oceanic lithosphere beneath Apulia, between late Jurassic and early Tertiary [e.g., *Agard et al.*, 2002; *Lombardo et al.*, 2002]. The rocks in the area are divided from west to east into three tectono-metamorphic blocks, forming a west-dipping nappe structure: the Queyras Schistes Lustrés complex, the eclogitic Monviso massif, and the UHP Dora Maira complex to the east (Figure 1b). The Queyras Schistes Lustrés complex is composed of kilometer-scale slices of meta-ophiolites embedded within the voluminous Mesozoic metasedimentary rocks [e.g., *Blake et al.*, 1995]. The complex shows a record of increasing metamorphic pressures and temperatures from lawsonite-blueschist facies in the western part to a transition between zoisite-blueschist and eclogite facies in the eastern part [*Caby*, 1996; *Agard et al.*, 2001]. The structurally underlying Monviso massif contains voluminous omphacite-bearing metavolcanic and metagabbroic rocks with minor (<20 vol%) metasedimentary rocks [*Schwartz et al.*, 2001]. Eclogites occur as
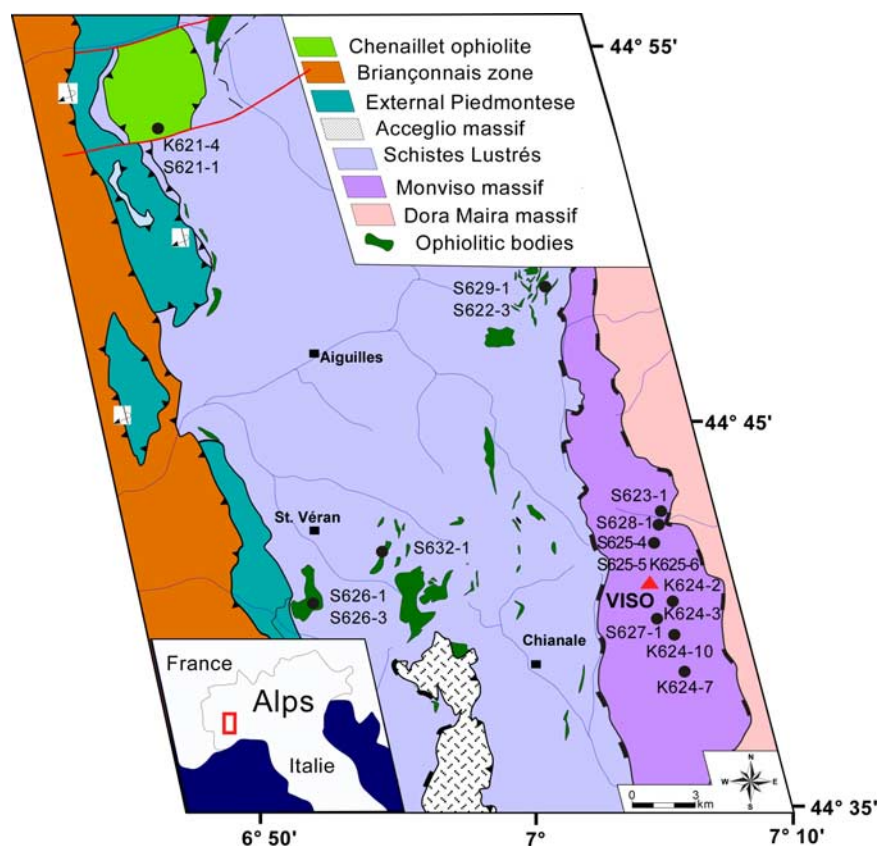
Figure 1b. Geological map of southwestern Alps showing serpentinite sample locations (solid circles) in the Chenaillet ophiolite, Schistes Lustrés, and Monviso massif. Towns and villages are shown with solid squares. Map modified after *Lardeaux et al.* [2006].

boudins in a matrix of serpentinites or highly deformed meta-basalts in mélange. The calculated metamorphic pressures and temperatures vary among different boudins in the serpentinites, suggesting that different boudins correspond to different blocks of oceanic crust that were subducted to different depths [*Blake et al.*, 1995]. The nappe structure, including the Dora Maira massif, is overlain by the Chenaillet ophiolite massif, which represents an obducted portion of the Tethyan oceanic crust. Therefore the Chenaillet massif escaped the Alpine metamorphism that affected all rocks in the underlying nappe structure.

[8] Serpentinites are abundant, constituting ~40 vol% of the entire area [*Schwartz et al.*, 2001]. Serpentinite samples were collected from the Chenaillet massif (S621-1, K621-4), Queyras Schistes Lustrés (S622-3, S626-1, S626-3, S629-1, S632-1) and Monviso massif (S623-1, K624-2, K624-3, K624-7, K624-10, S625-4, S625-5, K625-6, S627-1, S628-1).

2.3. Cuba

[9] Cuba is located in the northern part of the extinct Greater Antilles volcanic arc. Formation of the island started with development of an early Cretaceous arc on the southern margin of the North American plate in response to eastward subduction of the Farallon plate in the Pacific Ocean. A polarity reversal of subduction took place in Aptian-Albian time and the southward subduction of the Proto-Caribbean oceanic plate resulted in formation of the late Cretaceous arc on the northern margin of the Caribbean plate [*Hutson et al.*, 1998]. Our serpentinite samples were collected from the Zaza zone and Escambray massif in the central Cuba (Figure 1c). The Zaza zone is essentially a large mélange, a mixture of lenses and fragments of eclogitic basalts and gabbros plus deformed serpentinites [*Piotrowska*, 1993]. It represents an accretionary prism developed north of the late Cretaceous arc during the southward subduction of the Proto-Caribbean oceanic plate, that
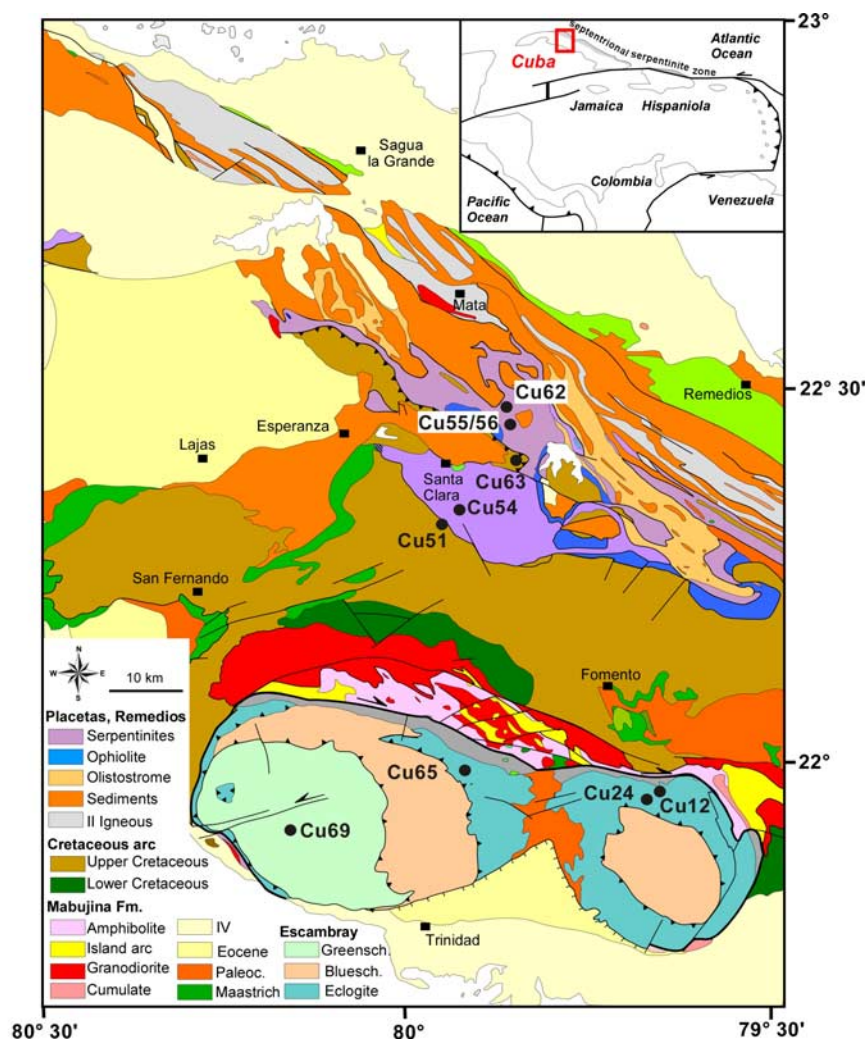
Figure 1c. Geological map of the central part of Cuba showing serpentinite sample locations (solid circles) in the Zaza zone, Cretaceous arc, and Escambray massif. Towns and villages are shown with solid squares. Map modified after *Millán* [1993].

formed at a slow-spreading Proto-Caribbean ridge [*Pindell et al.*, 1988].

[10] The Escambray massif is an accretionary prism developed in a forearc of the Cretaceous Caribbean "Great Arc" [*Burke*, 1988; *Pindell et al.*, 2005] during the subduction of the Farallon oceanic plate [e.g., *Hutson et al.*, 1998; *Schneider et al.*, 2004; *Stanek et al.*, 2006]. The massif is a mélange composed of metasedimentary rocks, lenses of serpentinites several hundred meters in length, and metamorphosed basalts (Figure 1c) [*Schneider et al.*, 2004; *Stanek et al.*, 2006]. *Millán* [1997] identified three nappes in the massif, with increasing metamorphic grade toward the north: greenschist facies, lawsonite-blueschist facies and zoisite-eclogite facies (Figure 1c).

[11] Samples (Cu54, Cu55, Cu56, Cu62) were collected from the eclogite-bearing serpentinite mélange in the Zaza zone, whereas other samples (Cu51, Cu63) came from the deformation zone between the Zaza zone and the base of the Cretaceous arc to the north (Figure 1c). In the Escambray massif, samples (Cu12, Cu24, Cu65) were collected from the zoisite-eclogitic facies nappe, and sample Cu69 came from the greenschist-facies nappe (Figure 1c).

3. Analytical Procedures

3.1. Bulk Rock Composition

[12] Hand specimens were washed with Milli-Q water after removing weathered surfaces. After

crushing the samples into small fragments, <2 cm, clean pieces that were free of cracks and veins were handpicked. These samples were again washed with Milli-Q water before grinding in a ceramic dish. Major and minor element concentrations were determined using a Philips PW 2400 X-ray fluorescent spectrometer at the University of Ottawa. Replicate runs of rock references (MRG-1, Sy-2, JP-1) indicate an accuracy and precision of <0.8% for major elements and 10% for minor elements, in terms of quoted values. The concentrations of Rb, Sr and Pb were determined by isotopic dilution using mixed spike solutions of ^{87}Rb-^{84}Sr, ^{148}Nd-^{149}Sm, and ^{208}Pb, which were added to the samples before digestion with HF-HNO$_3$ mixture; each element was separated following the standard resin technique. Isotopic ratio measurements of Rb and Sr were made with an Agilent HP 4500 ICP-MS at the University of Ottawa.

[13] Platinum-group element concentrations were determined by isotopic dilution using a mixed spike of ^{101}Ru, ^{105}Pd, ^{190}Os, ^{191}Ir, and ^{194}Pt; the isotope ratios were determined with an Agilent HP 4500 ICP-MS at the University of Ottawa. The analytical procedure is essentially identical to that discussed by *Ravizza and Pyle* [1997]. Blank contributions were 0.002–0.004 ng Ru/g flux, 0.002–0.007 ng Ir/g flux, 0.002–0.006 ng Os/g flux, 0.07–0.16 ng Pt/g flux and 0.03–0.12 ng Pd/g flux, negligible compared to the sample amounts; thus blank corrections were not applied to the results.

3.2. Mineral Compositions

[14] Mineral compositions were determined using a Cameca CAMEBAX SX100 microprobe with count time of 10 s/element, 20 kV accelerating potential and 20 nA sample current. Standards used were albite (Si), MgO (Mg), Al$_2$O$_3$ (Al), Cr$_2$O$_3$ (Cr), Fe$_2$O$_3$ (Fe), TiMnO$_3$ (Ti, Mn), vanadinite (V), NiO (Ni) and Co metal (Co). The Fe$_2$O$_3$ contents of spinel were calculated assuming a stoichiometric composition. Sulphide minerals were identified using JEOL 6400 digital scanning electron microscope equipped with a 40° take-off angle and a Link X-ray analyzer.

3.3. Strontium Isotope Compositions

[15] For Sr isotopic analysis, samples were dissolved using HF-HNO$_3$ (5:1) in Savillex screw-top Teflon vials at 180°C for >24 hrs. After repeatedly

drying and dissolving the residue in HCl, the sample was loaded in 2.5 N HCl on cation resin (Bio Rad AG 50 W-X8, 200–400 mesh) and Sr was eluted with 2.5 N HCl [*Hart and Brooks*, 1977]. Total chemical blanks are less than 0.05 ng for Sr, negligible in comparison to the amount of Sr in samples. HCl was double distilled in Savillex Teflon distillation vessels at sub-boiling temperatures. Double distilled HF and HNO$_3$ were purchased from Seastar Chemicals, British Columbia.

[16] Isotopic measurements were made on a multi-collector thermal ionization mass spectrometer (Finnigan MAT 261) at Carleton University in Ottawa, and the ratios for Sr were normalized to ^{86}Sr/^{88}Sr of 0.1194. NBS987 ^{87}Sr/^{86}Sr was 0.710257 ± 0.000014.

3.4. Sulphur Isotopes

[17] Total sulphur was extracted as H$_2$S from approximately 30–35 g bulk rock by reacting the samples with KIBA [*Sasaki et al.*, 1979] in a Pyrex flask. The H$_2$S was precipitated as Ag$_2$S and the weight of Ag$_2$S was used to calculate the concentration of total S in the samples. For sulphur isotope analysis, the Ag$_2$S was mixed with V$_2$O$_5$ (1:2 weight ratio) in Al foil and placed in a Carlo Erba 1110 elemental analyzer to yield SO$_2$ at 1700°C. The SO$_2$ gas was introduced to a Finnigan-Mat Delta Plus mass spectrometer at the University of Ottawa after passing through 7 mL of silica at 1000°C and Cu at 600°C. The analytical procedure is essentially identical to that described by *Hattori et al.* [2004].

4. Petrology

[18] Serpentinites from the Himalayas consist mainly of antigorite and spinel with minor chlorite, talc and secondary olivine (Figures 2a and 2b). The secondary olivine replaces antigorite and commonly contains inclusions of magnetite and antigorite (Figure 2a); it is characterized by high Mg (Fo > 96; Table 1a), which is too high to be primary olivine (Fo < 94) in mantle peridotites. Primary chromite grains are almost always rimmed by ferritchromite and magnetite (Figure 2b). Sulphide minerals are extremely rare, but very small (<5 μm) grains of millerite (NiS) and heazlewoodite (Ni$_3$S$_2$) were identified. Serpentinites from the Alps and Cuba also contain antigorite as the predominant serpentine mineral and minor chrysotile, lizardite,
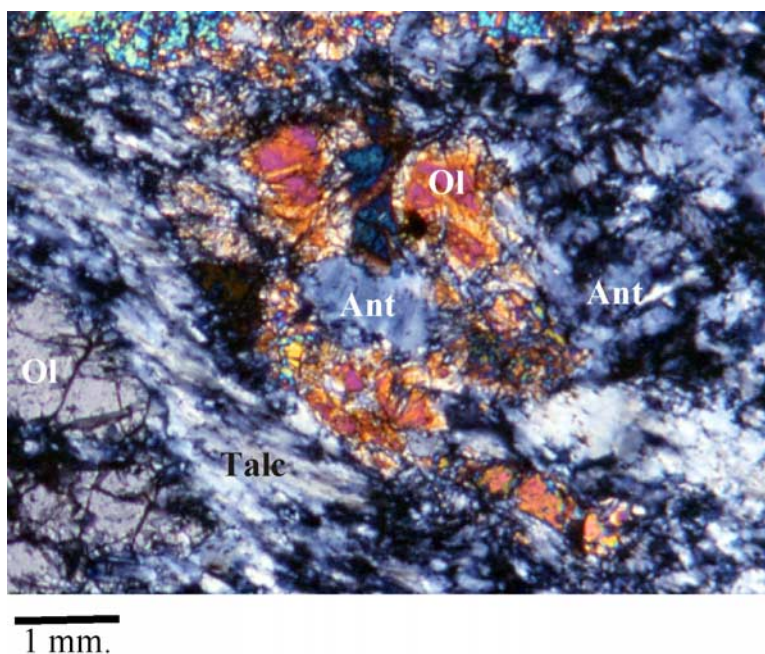
1 mm.

Figure 2a. Photomicrograph showing the secondary olivine (Ol) replacing antigorite (Ant) in serpentinite (sample CH 98b). The secondary olivine commonly contains antigorite and magnetite inclusions and is characterized by high Mg (Fo > 96; Table 4c), which is clearly different from olivine in anhydrous mantle peridotites (Fo < 94).

talc, chlorite and magnetite. No primary minerals were identified in Alpine serpentinites and all oxides are magnetite. Most serpentinite samples from Cuba are similar to Alpine samples with no primary minerals, except for three samples. Sample Cu 55 contains relict clinopyroxene, orthopyroxene and olivine (Fo 90.5, Table 1a); samples Cu51 and Cu63 from the deformation zone contain chromite grains rimmed by magnetite, similar to Himalayan serpentinites. Sulphide minerals, mostly pyrrhotite and pentlandite, occur in Alpine serpentinites, but not in Cuban samples.

4.1. Serpentine Minerals

[19] Antigorite is the major serpentine mineral in all samples. The predominant occurrence of antigorite as a serpentine mineral in our samples is consistent with the close association of samples with eclogites in the field, as described in the geological settings, because antigorite is the high-temperature phase of serpentine minerals [*Evans*, 1977; *Wünder et al.*, 2001]. Antigorite commonly forms blades instead of pseudomorphs of silicate minerals, but the relict olivine grains can be distinguished in some samples, as the original grains are outlined by dusty magnetite. Serpentinized

orthopyroxene grains are recognized in magnetite-free areas of antigorite in several samples.

[20] Himalayan samples contain rare veinlets of lizardite in the matrix of antigorite. This cross-cutting relationship suggests that the lizardite formed later at lower temperatures. On the other hand, Cuban and Alpine samples show evidence
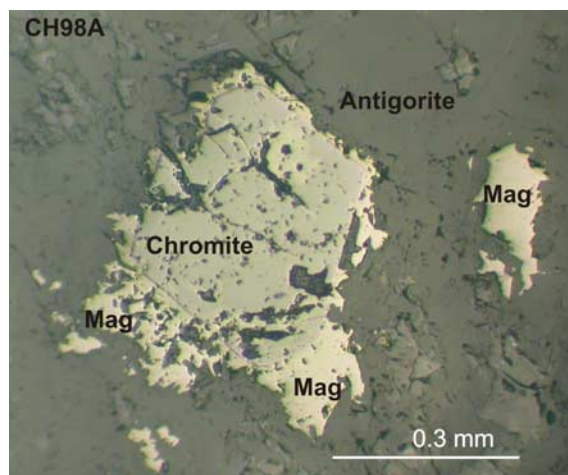

Figure 2b. Photomicrograph of chromite rimmed by magnetite (Mag), surrounded by antigorite, under open polarized incident light (Sample CH 98A).

Table 1a. Compositions of Representative Olivine Grains

Areas Remark	CH98b[a] Himalayas Secondary	CH98b[a] Himalayas Secondary	CH430 Himalayas Secondary	CH423 Himalayas Secondary	Cu55 Cuba Primary	Cu55 Cuba Primary
SiO_2	42.73	42.67	43.45	42.56	41.27	41.17
TiO_2	0.04	0.04	0.00	0.04	0.04	0.02
FeO	3.95	3.81	2.05	2.12	9.27	9.00
MgO	54.83	54.78	54.12	54.99	49.34	49.4
MnO	0.25	0.16	0.16	0.14	0.048	0.189
Cr_2O_3	<0.02	<0.02	<0.02	<0.02	<0.01	0.054
NiO	<0.02	<0.02	<0.02	<0.02	0.39	0.38
Total	101.8	1.1.4	99.79	99.87	100.4	100.2
Si	1.00	1.00	1.02	1.00	1.00	1.00
Ti	0.00	0.00	0.00	0.00	001	0.00
Fe	0.08	0.07	0.05	0.04	0.189	0.184
Mg	1.91	1.92	1.91	1.94	1.791	1.795
Mn	0.00	0.00	0.00	0.00	0.001	0.004
Cr	0.00	0.00	0.00	0.00	0.000	0.001
Ni	0.00	0.00	0.00	0.00	0.008	0.008
Fo,[b] %	96.1	96.3	97.9	97.9	90.5	90.7

[a] Olivine grains in CH98b replace antigorite, as shown in Figure 2a.
[b] Fo is the forsterite component, $100*(Mg/[Mg + Fe])$.

for the early formation of lizardite. A detailed micro-Raman study combined with transmission electron microscopy of serpentinite samples by *Auzende et al.* [2002, 2006] found minor lizardite along cracks of silicate minerals, surrounded by antigorite in Cuban samples Cu12 and Cu55 (Figure 3) and Alpine sample K624-2. A similar occurrence of lizardite and cross-cutting antigorite was also observed in an Alpine sample (S626-11) during this study. Lizardite is a low-temperature phase of serpentine minerals [e.g., *Evans*, 1977] and is cut by antigorite in the Cuban and Alpine

Table 1b. Compositions of Representative Spinel Grains From the Himalayas

	CH35a	CH98a	CH98b	CH146	CH187	CH187	CH422	CH423	CH430	CH433
SiO_2	0.03	<0.02	<0.02	<0.02	0.04	0.04	0.06	0.05	<0.02	0.05
MgO	7.88	6.74	7.72	6.32	4.57	7.42	5.79	6.05	7.08	8.77
Al_2O_3	18.80	8.82	9.29	7.39	4.45	9.82	11.31	7.45	9.26	18.10
TiO_2	0.10	0.04	0.04	0.13	0.05	0.07	0.11	0.15	0.58	0.12
Cr_2O_3	42.67	57.07	58.74	53.49	21.10	55.90	53.08	54.84	50.21	47.51
NiO	0.09	0.03	0.05	0.08	0.43	0.00	0.05	0.04	0.12	0.06
MnO	0.68	0.00	0.00	0.00	0.94	0.00	0.49	0.81	0.25	0.40
FeO	21.45	22.90	21.70	23.17	22.53	21.98	22.59	22.77	16.58	20.90
Fe_2O_3	7.33	3.82	2.92	8.92	42.78	4.48	5.79	7.71	10.49	4.09
Sum	99.03	99.44	100.5	99.50	96.88	99.71	100.4	100.4	99.89	100.0
Al	5.77	2.85	2.94	2.41	1.55	3.13	3.57	2.42	2.96	5.50
Cr	8.78	12.36	12.46	11.69	4.93	11.95	11.24	11.95	10.78	9.68
Fe^{3+}	1.44	0.79	0.59	1.85	9.50	0.91	1.17	1.60	2.14	0.79
Ti^{4+}	0.00	0.01	0.01	0.03	0.01	0.01	0.02	0.03	0.12	0.02
Fe^{2+}	4.77	5.24	4.87	5.35	5.56	4.97	5.06	5.25	3.76	4.51
Mg^{2+}	3.06	2.75	3.09	2.59	2.01	2.99	2.74	2.48	2.87	3.37
Mn^{2+}	0.15	0.00	0.00	0.00	0.24	0.00	0.11	0.19	0.96	0.09
Ni^{2+}	0.02	0.01	0.01	0.02	0.10	0.00	0.01	0.01	0.02	0.01
Cr#	0.60	0.81	0.81	0.83	0.76	0.80	0.76	0.83	0.78	0.64
Mg#*	0.39	0.34	0.39	0.33	0.27	0.38	0.35	0.32	0.43	0.43

Table 1c. Compositions of Representative Spinel Grains From Cuba

	Cu51	Cu51	Cu63	Cu63	Cu63
SiO_2	0.03	0.04	0.05	<0.02	<0.02
MgO	12.55	11.70	12.28	11.68	11.95
Al_2O_3	31.37	30.76	22.91	23.54	22.73
TiO_2	0.04	0.02	0.06	0.02	0.07
Cr_2O_3	37.51	37.77	42.24	41.60	43.03
NiO	0.06	0.12	0.07	0.12	0.06
MnO	0.19	0.25	0.27	0.33	0.21
FeO	17.64	18.60	16.15	17.36	16.71
Fe_2O_3	0.92	0.63	4.98	5.26	4.21
Sum	100.3	99.89	99.01	99.94	98.97
Al	8.78	8.71	6.73	6.87	6.69
Cr	7.04	7.17	8.32	8.14	8.50
Fe^{3+}	0.16	0.11	0.93	0.98	0.79
Ti^{4+}	0.01	0.00	0.01	0.00	0.01
Fe^{2+}	3.50	3.74	3.37	3.59	3.49
Mg^{2+}	4.44	4.19	4.56	4.31	4.45
Mn^{2+}	0.04	0.05	0.06	0.07	0.04
Ni^{2+}	0.01	0.02	0.01	0.02	0.01
Cr#	0.45	0.45	0.55	0.54	0.56
Mg#[a]	0.56	0.53	0.58	0.55	0.56

[a] Mg# is atomic ratios of $Mg/(Mg + Fe^{2+})$.

samples (Figure 3). Such textural evidence indicates that peridotites in the Alps and Cuba underwent early hydration at low temperatures, with a later heating event to form the antigorite.

4.2. Spinel Composition

[21] Chromian spinel is extensively oxidized to ferritchromite and magnetite (Figure 1c), but the cores of chromite grains in all Himalayan samples retain their primary compositions, judging from low Fe^{3+} ($Fe^{3+}/[Fe^{3+} + Al + Cr^{3+}] < 0.12$), and TiO_2 (<0.22 wt%; Table 1b). The relict nature of the cores is further supported by similar compositions in different grains in individual samples. The spinel grains from the Himalayan samples contain high Cr (Cr# = atomic ratios of Cr/[Cr + Al], 0.76–0.83). High Cr# values confirm the refractory nature of the protoliths of our serpentinites, because Al is preferentially incorporated into melt during partial melting. Himalayan serpentinites plot in a field similar to those from the Mariana forearc serpentinites, in the spinel ternary diagram of trivalent cations (Figure 4) and also in the binary diagram of Cr# and Mg# ($Mg/[Mg + Fe^{2+}]$).

[22] Alpine samples have been extensively and pervasively oxidized, and Cr-spinel grains are all converted to Cr-bearing magnetite. Spinel grains from Cuban samples are also oxidized to magnetite. Sample Cu 55 contains relict primary olivine and pyroxenes, but chromite grains are all porous and oxidized to magnetite. Relic chromite grains were found only in two samples, Cu51 and Cu63
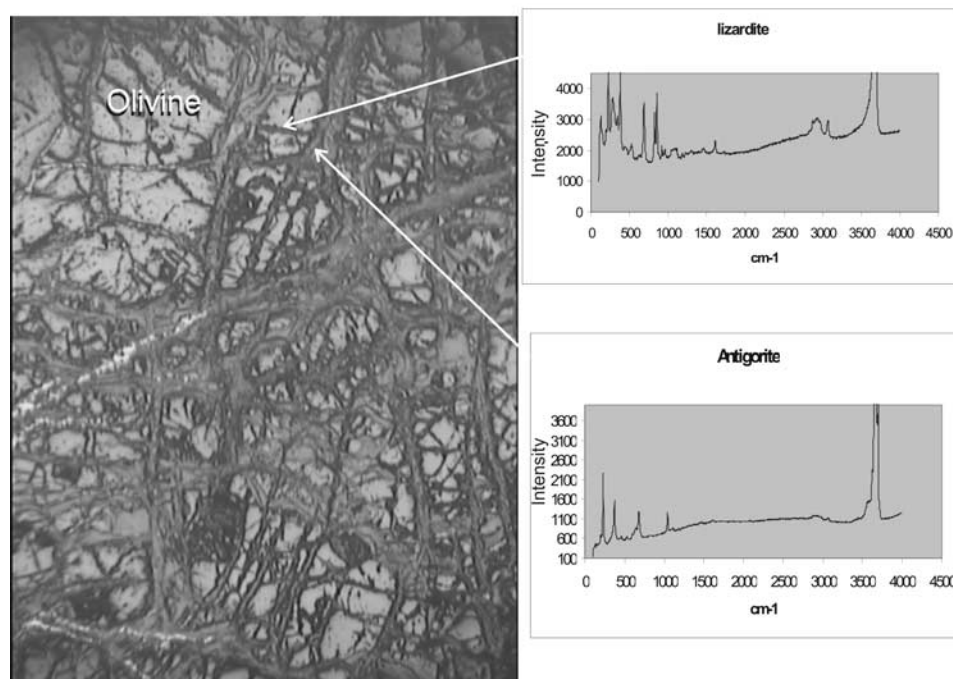

Figure 3. Micro-Raman spectroscopy identification of serpentine minerals. Sample Cu55 from Cuba. Cracks of olivine grains are filled by lizardite, surrounded by antigorite, suggesting that lizardite formed earlier at lower temperature and that antigorite formed later at higher temperature.
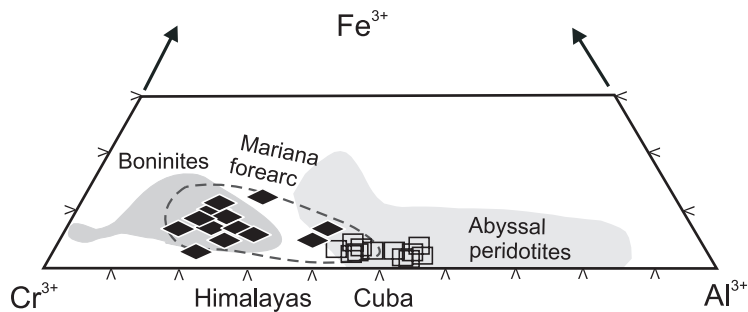
Figure 4. Ternary trivalent cation plot of cores of chromite grains in the serpentinites from Himalaya (solid flat diamonds) and Cuba (open squares). Each point represents one spinel grain. Himalayan samples include CH98A, CH 98B, CH146, CH187, and CH422, and Cuban samples are Cu51 and Cu63. Chromite grains in other Cuban samples and all Alps samples are oxidized to ferritchromite and magnetite; their compositions are not plotted. The field of Mariana forearc peridotites, shown by the dashed line, is from *Ishii et al.* [1992] and *Parkinson and Pearce* [1998]. The fields for abyssal peridotites and boninites are from *Dick and Bullen* [1984] and *Barnes and Roeder* [2001], respectively. The compositions of chromite from the MARK region, mid-Atlantic ridge, are reported by *Burgath et al.* [1997], but the compositions plot within the field for abyssal peridotites.

(Table 1c). These samples were collected from the deformation zone between the highest metamorphic grade of the Zaza zone and the base of the arc igneous complex in Cuba (Figure 1c), and have a similar texture of the chromite grains in the Himalayan samples. The cores show moderate Cr#, ranging from 0.42 to 0.56 (Figure 4 and Table 1c). Significant amounts of Al in chromite grains suggest an undepleted nature of the protoliths of the serpentinites. Indeed, they plot in the area for less refractory forearc mantle peridotites and also in the refractory part of abyssal peridotites [*Dick and Bullen*, 1984] (Figure 4).

5. Results

5.1. Major Elements

[23] Bulk rock compositions of most samples contain high MgO (30–42 wt%), Cr (>2000 ppm) and Ni (>2000 ppm), and low Al_2O_3 (0.31–2.8 wt%; Tables 2a, 2b, and 2c). In terms of Mg/Si versus Al/Si, most samples show lower Al/Si than primitive mantle values (Figure 5a). The data suggest that the samples are refractory peridotite residues after partial melting, because Al is mildly incompatible with mantle minerals and is depleted during partial melting. Several samples show distinctly higher Al_2O_3 values than primitive mantle value (Figure 5a and Tables 2a, 2b, and 2c); for example, the Al_2O_3 contents in Cu69, Cu62, and S621-1 are 20.7, 7.7, and 13 wt%, respectively. These samples also contain high CaO (3–15 wt%) and low Cr (<400 ppm) and Ni (<400 ppm). Since, CaO is preferentially removed during the partial melting in

the mantle, the high Ca and Al suggest that these samples are ultramafic cumulates.

[24] Compared to the other serpentinite samples, the Himalayan samples are the most refractory serpentinites, with high MgO (>36 wt%) and low Al_2O_3 (<1.2 wt%; Table 2a); they plot in a vertical array on the Mg/Si versus Al/Si diagram (Figure 5b). The observed vertical array at a low Al/Si ratio suggests that they are derived from a highly refractory mantle, since Si is removed from peridotites after Al during partial melting. The vertical array displayed by Himalayan samples is similar to that for the Mariana forearc serpentinites (Figure 5b).

[25] Alpine serpentinites contain generally higher Al than Himalayan samples (Figure 5b and Table 2c), suggesting that the Alpine samples are less refractory. Alpine samples plot in the area for abyssal peridotites (Figure 5b), and also show district-scale compositional variations, suggesting that different nappes originated from different mantle domains. Serpentinites from the Monviso massif in the Alps contain low Al/Si and plot in a narrow area on a Mg/Si versus Al/Si diagram (Figure 5b). They show similar compositions to those for average abyssal peridotites, and are comparable in composition to those of hydrated harzburgites recovered from the MARK region of the Mid-Atlantic Ocean ridge (Figure 5b). On the other hand, serpentinites from the Chenaillet ophiolite massif in the Alps show higher Al/Si, even less refractory than the Monviso samples (Figure 5b). Comparing the Chenaillet samples with abyssal peridotites, the former plot in the least refractory

Table 2a. Bulk Rock Chemical Compositions of Samples From the Himalayas[a]

	Analytical Method[b]	CH 98a	CH98b	CH146	CH 187	CH422	CH423	CH430	CH432	CH433	CH35a	TS18C	CH52C
Location[c] / Protolith[d]		Zildat wedge 33°13'	Zildat wedge 33°13'	Zildat wedge 33°09'	Zildat wedge 33°14'	Zildat wedge 33°14'	Zildat wedge 33°14'	Zildat wedge 33°13'	Zildat wedge 33°13'	Zildat wedge 33°13'	Nidar cumu 33°15'	Nidar cumu 33°15'	Drakka cumu 33°15'
Latitude		26.32 N 78°22'	26.32 N 78°22'	59.97 N 78°25'	12.02 N 78°21'	12.02 N 78°21'	12.02 N 78°21'	26.32 N 78°22'	26.32 N 78°22'	26.32 N 78°22'	21.22 N 78°24'	16.81 N 78°26'	21.48 N 78°24'
Longitude		17.16 E	17.16 E	08.76 E	43.78 E	43.78 E	43.78 E	17.16 E	17.16 E	17.16 E	10.86 E	26.87 E	04.02 E
SiO_2	XRF	35.1	40.2	40.6	39.4	39.6	37.4	43.2	39.4	39.2	38.7	38.1	29.6
TiO_2	XRF	0.03	0.015	0.02	0.02	0.02	0.008	0.044	0.013	0.01	0.02	0.032	0.37
Al_2O_3	XRF	0.54	0.37	0.77	1.09	1.6	0.31	2.53	1.18	0.56	0.49	8.44	16.7
Fe_2O_3 (t)	XRF	6.83	7.54	7.59	8.99	7.99	6.60	7.29	7.58	7.39	7.58	8.19	5.55
MnO	XRF	0.13	0.10	0.09	0.11	0.089	0.125	0.060	0.081	0.10	0.1	0.11	0.28
MgO	XRF	40.0	41.8	36.7	38.0	37.0	41.9	34.3	37.8	37.5	38.6	30.6	29.7
CaO	XRF	0.64	0.29	1.05	0.33	0.482	0.201	0.45	0.64	1.4	0.65	3.22	4.41
Na_2O	XRF	<0.005	<0.005	<0.005	<0.005	<0.005	<0.005	<0.005	<0.005	<0.005	<0.005	0.16	<0.005
K_2O	XRF	<0.005	<0.005	<0.005	<0.005	<0.005	<0.005	0.002	<0.005	<0.005	<0.005	0.005	0.03
P_2O_5	XRF	0.005	0.006	<0.002	<0.002	0.005	0.024	0.008	0.009	0.006	0.081	0.03	0.081
LOI	XRF	16.4	9.8	13.7	11.6	13.1	13.2	11.6	12.8	13.5	13.8	11.1	14.7
Cr	XRF	2720	2600	2580	2780	2290	768	2640	2160	2370	2120	3160	32
Ni	XRF	2260	2830	2260	2390	2060	2760	2290	1850	1980	2220	1390	16
Nb	ICP-MS	0.82	0.56	0.07	0.06	0.98	0.37	0.4	0.07	0.14	0.84	n.d.	n.d.
Rb	ID	0.08	0.07	0.033	0.11	0.10	0.11	0.32	0.04	0.14	1.0	n.d.	n.d.
Sr	ID/XRF	23	13	30	6.9	9	7	20	19	55	10	36	28
Ce	ICP-MS	0.38	0.41	0.12	0.09	0.28	0.17	0.66	0.22	0.54	0.29	n.d.	n.d.
Nd	ID	0.058	0.076	0.049	0.041	0.131	0.1	n.d.	n.d.	0.152	n.d.	n.d.	n.d.
Sm	ID	0.019	0.021	0.019	0.019	0.04	0.03	n.d.	n.d.	0.041	n.d.	n.d.	n.d.
Zr	ICP-MS	0.2	0.4	0.3	0.2	0.2	0.3	0.5	0.2	0.2	0.2	0.3	69
Sc	ICP-MS	5.3	3.8	5.7	7.9	11	3.2	14	13	5.5	5.3	11	n.d.
Y	ICP-MS	0.4	0.5	0.4	0.7	0.6	0.3	1.1	0.4	0.4	0.5	2	29
Pb	ICP-MS	14	2.6	7.8	34	2.15	2.44	1.8	1.5	2.0	19	19	n.d.
As	H-AA	275	54	6.0	145	27	49	48	55	62	56	2.8	n.d.
Sb	H-AA	12	10	0.69	10.2	1.3	7.25	3.6	6.2	4.7	6.4	<0.1	n.d.
Total		100.1	101.3	100.5	101.7	100.0	100.7	100.2	101.5	100.3	100.4	100.6	101.4

[a] Oxides and LOI (loss of ignition) are expressed in wt.%; others are in ppm. Total Fe was expressed as Fe_2O_3 (t). LOI was determined after heating 2 g samples for >1 hr at 1050 C. n.d., not determined.
[b] XRF, Philips PW-2400 X-ray fluorescence spectrometer; ID, isotopic dilution; ICP-MS, inductively coupled plasma mass spectrometer; H-AA, atomic absorption spectrometer attached to a hydride generator.
[c] Drakk, mélange in Drakkarpo unit; Nidar, base of the Nidar arc ophiolite complex (Figure 1a).
[d] Protolith: abyss, abyssal peridotites; cumu, cumulates; wedge, forearc mantle wedge peridotites.

Table 2b. Bulk Rock Chemical Compositions of Samples From Cuba

	Analytical Method	Cu12	Cu24	Cu 51	Cu 54	Cu55	Cu56	Cu62	Cu63	Cu65	Cu69
Location[a]		Escam	Escam	Def. Z.	Zaza	Zaza	Zaza	Zaza	Def. Z.	Escam	Escam
Protolith[b]		abyss	abyss	wedge	abyss	abyss	abyss	abyss	wedge	cumu	cumu
Latitude		21°59' 18.99 N	21°59' 02.24 N	22°18' 06.78 N	22°20' 27.11 N	22°41' 11.85 N	22°20' 27.11 N	22°32' 21.36 N	22°24' 20.12 N	21°59' 15.87 N	21°56' 41.98 N
Longitude		79°41' 15.21 W	79°42' 45.44 W	79°59' 00.63 W	79°57' 30.82 W	79°53' 55.07 W	79°57' 30.82 W	79°49' 55.30 W	79°52' 59.83 W	79°51' 52.55 W	80°04' 35.20 W
SiO_2	XRF	39.6	43.4	40.8	42.2	41.4	38.9	43.5	39.7	41.2	27.8
TiO_2	XRF	0.07	0.073	0.008	0.039	0.058	0.049	0.017	0.009	0.018	1.00
Al_2O_3	XRF	2.62	1.74	0.78	1.74	2.16	2.15	7.68	0.57	3.01	20.7
Fe_2O_3 (t)	XRF	8.42	8.91	7.76	8.21	8.11	9.15	7.16	8.22	9.74	15.34
MnO	XRF	0.12	0.14	0.10	0.11	0.12	0.10	0.09	0.09	0.12	0.34
MgO	XRF	36.4	32.9	35.4	35.3	38.6	35.4	26.8	36.9	34.0	23.7
CaO	XRF	0.08	0.92	0.19	0.06	3.17	0.10	5.60	0.05	0.08	0.75
Na_2O	XRF	<0.005	<0.005	<0.005	<0.005	0.03	<0.005	0.34	<0.005	<0.005	<0.005
K_2O	XRF	<0.005	<0.005	<0.005	<0.005	0.036	<0.005	0.037	<0.005	<0.005	<0.005
P_2O_5	XRF	0.007	0.006	0.007	0.004	0.005	0.005	0.008	0.008	0.004	0.029
LOI		12.5	11.4	14.5	11.9	6.1	13.7	8.1	14	12.3	11.9
Cr	XRF	2320	2400	2680	2110	2400	2930	1800	2530	2470	361
Ni	XRF	1750	1930	2190	1580	2000	2340	1610	3620	2060	338
Rb	ID	0.08	0.052	0.085	0.1	0.5	0.057	0.22	0.14	n.d.	0.28
Sr	ID	1.0	0.73	1.6	4.1	1.4	1.1	11	2	1	5.1
Ce	ICP-MS	2.2	0.67	<0.06	0.58	0.04	0.05	0.42	0.08	0.13	4.3
Nd	ID	n.d.	0.45	0.045	0.124	n.d.	n.d.	1.00	0.051	n.d.	4.8
Sm	ID	n.d.	0.11	0.042	0.085	n.d.	n.d.	0.67	0.009	n.d.	2.5
Zr	ICP-MS	1.2	0.65	<0.2	0.3	0.6	0.3	0.4	0.2	0.3	7.6
Sc	ICP-MS	14	13	11	7.7	14	13	16	8.2	13	73
Y	ICP-MS	1.5	2.5	<0.1	1.2	2.0	1.0	5.6	0.1	1.2	41
Pb	ICP-MS	0.74	1.4	1.5	1.9	0.15	0.43	0.6	0.67	0.13	0.64
As	H-AA	1.7	0.3	2.1	3.8	2	2.1	1.1	2.6	2.8	0.6
Sb	H-AA	0.04	0.08	0.06	0.14	<0.03	0.05	0.07	<0.03	0.09	<0.03
Total		100.4	100.1	100.3	100.2	100.5	100.4	99.9	100.6	101.2	101.7

[a] Escam, Escambray massif in Cuba; Def Z, major deformation zone between the highest metamorphic grade rocks of the Zaza zone and the base of arc volcanic rocks in Cuba.
[b] Protolith: abyss, abyssal peridotites; cumu, cumulates; wedge, forearc mantle wedge peridotites.

Table 2c. Bulk Rock Chemical Compositions of Samples From the Alps[a]

	Analytical Method	K621-4	K622-3	K623-1	K624-2	K624-3	K624-7	K624-10	S625-4	S626-1	S626-3	S627-1	S628-1	S629-1	S-632-1	S621-1	S625-5	K625-6
Location[b]		Chena	Lustrés	Viso	Viso	Viso	Viso	Viso	Viso	Lustrés	Lustrés	Viso	Viso	Lustrés	Lustrés	Chena	Viso	Viso
Protolith[c]		abyss	abyss	abyss	abyss	abyss	abyss	abyss	abyss	abyss	abyss	abyss	abyss	abyss	abyss	cumu	cumu	cumu
Latitude		44°52′ 53.23 N	44°49′ 11.57 N	44°42′ 20.69 N	44°39′ 17.29 N	44°39′ 17.29 N	44°38′ 19.21 N	44°38′ 48.01 N	44°41′ 48.83 N	44°38′ 22.88 N	44°38′ 20.62 N	44°38′ 51.71 N	44°42′ 00.12 N	44°49′ 11.47 N	44°49′ 33.01 N	44°52′ 53.23 N	44°41′ 48.83 N	44°41′ 48.83 N
Longitude		06°43′ 54.78 E	07°01′ 11.49 E	07°04′ 26.75 E	07°07′ 30.22 E	07°07′ 30.22 E	07°07′ 27.06 E	07°06′ 59.39 E	07°05′ 22.44 E	06°53′ 31.07 E	07°01′ 03.92 E	07°08′ 28.10 E	07°05′ 23.17 E	07°01′ 03.85 E	06°55′ 57.35 E	06°43′ 54.78 E	07°05′ 22.44 E	07°05′ 22.44 E
SiO_2	XRF	41.2	47.1	40.99	40.4	40.1	40.4	40.3	41.5	39.3	37.8	40.1	41.1	39.8	38.4	39.7	47.8	34.9
TiO_2	XRF	0.063	0.103	0.016	0.014	0.024	0.013	0.015	0.027	0.038	0.031	0.016	0.013	0.03	0.027	1.34	1.13	1.14
Al_2O_3	XRF	2.29	2.73	1.47	1.49	1.57	1.49	1.33	1.78	1.42	1.36	1.51	1.58	2.87	1.29	13.7	15.3	6.53
Fe_2O_3 (t)	XRF	7.93	10.6	6.63	8.15	8.50	8.2	7.96	8.33	7.71	9.17	8.35	7.02	8.94	11.21	8.23	8.25	13.07
MnO	XRF	0.10	0.090	0.090	0.097	0.11	0.093	0.098	0.071	0.11	0.12	0.10	0.13	0.11	0.07	0.30	0.25	0.090
MgO	XRF	34.4	30.0	37.1	37.6	37.4	37.7	37.9	36.3	37.9	37.0	37.9	38.0	35.8	36.6	14.6	8.14	32.2
CaO	XRF	0.726	0.126	2.08	0.005	0.008	0.003	0.01	0.01	0.05	0.07	0.00	0.01	0.10	0.03	15.2	12.7	0.685
Na_2O	XRF	<0.005	0.005	<0.005	<0.005	<0.005	<0.005	<0.005	<0.005	<0.005	<0.005	<0.005	<0.005	<0.005	<0.005	<0.005	3.87	<0.005
K_2O	XRF	<0.005	<0.005	<0.005	<0.005	<0.005	<0.005	<0.005	<0.005	<0.005	<0.005	<0.005	<0.005	<0.005	<0.005	<0.005	0.251	<0.005
P_2O_5	XRF	0.006	0.004	0.005	0.004	0.004	0.005	0.004	0.005	0.013	0.013	0.006	0.007	0.005	0.006	0.16	0.076	0.508
LOI		12.6	9	12	11.8	11.9	11.8	12.1	11.7	13.3	13.6	11.8	12	12	12.9	6.9	1.8	11.3
Cr	XRF	2980	2860	2520	2740	3140	2140	2200	2130	1990	2910	2730	2250	2520	2620	201	273	1330
Ni	XRF	2040	2000	1210	2260	2230	2140	1960	2090	2100	2310	1800	1590	2030	2740	111	217	1800
Rb	ID	0.24	0.32	0.28	0.035	0.063	0.036	0.029	0.042	n.d.	0.064	0.018	0.019	0.15	0.073	0.3	8	0.028
Sr	ID	8	2.3	3.64	0.5	1.1	2.1	0.5	3.3	n.d.	0.93	0.5	0.5	2.5	2	37	193	13
Ce	ICP-MS	0.36	0.15	0.3	0.37	0.124	0.35	0.4	0.51	n.d.	0.088	0.43	0.37	0.19	0.4	13	16	4.1
Nd	ID	0.144	0.138	0.13	n.d.	0.228	0.276	0.153	n.d.	n.d.	0.113	n.d.	n.d.	0.24	0.26	n.d.	n.d.	5.3
Sm	ID	0.100	0.075	0.077	n.d.	0.11	0.085	0.042	n.d.	n.d.	0.044	n.d.	n.d.	0.145	0.064	n.d.	n.d.	2.0
Zr	ICP-MS	2	1	<1	<1	<1	1.4	<1	<1	n.d.	<1	<1	<1	<1	<1	120	94	150
Sc	ICP-MS	13	21	10	13	12	12	10	9.3	n.d.	9.8	11	10	14	5.7	29	n.d.	9.7
Y	ICP-MS	1.9	1.4	0.9	2.2	3.4	1.6	0.9	0.6	n.d.	1.0	1.4	1.3	2.7	0.6	28	27	13
Pb	ICP-MS	1.0	0.08	0.19	0.31	0.62	0.35	0.28	1.8	n.d.	0.53	0.26	1.6	0.86	0.76	0.41	n.d.	0.31
As	H-AA	1.7	0.4	0.4	2.4	0.1	0.2	2.3	3.4	n.d.	2.1	2.9	3.7	2.8	3.3	4.7	n.d.	0.6
Sb	H-AA	0.02	0.28	<0.01	0.04	0.03	0.04	0.04	0.07	n.d.	<0.02	0.06	0.07	0.44	0.54	0.02	n.d.	<0.02
Total		100.1	100.4	100.9	100.3	100.4	100.3	100.4	100.5	99.80	99.91	100.5	100.4	100.3	101.4	100.3	99.63	101.1

[a] Samples S621-1 and K621-4 were collected at the same location. K621-4 contains abundant pseudomorphs of orthopyroxene, whereas S621-1 is fine-grained with no relict textures.

[b] Chena, Chenaillet; Lustrés, Schistes Lustrés; Viso, Monviso.

[c] Protolith: abyss, abyssal peridotites; cumu, cumulates; wedge, forearc mantle wedge peridotites.

Table 2d. Contents of Platinum Group Elements[a]

	K621-4	S622-3	K624-2	K624-7	K624-10	S625-4	S626-3	S627-1	S628-1	S629-1	S632-1	S625-6 cumu[b]	Cu12	Cu24	Cu51	Cu54	Cu55	Cu56	Cu62	Cu63	Cu 69 cumu[b]
Os	3.6	2.0	3.1	2.1	6.5	1.6	3.4	2.4	2.9	3.0	3.4	0.18	1.7	2.0	3.4	1.8	3.4	1.8	1.9	2.5	0.05
Ir	3.9	2.5	3.3	2.1	4.5	1.4	3.4	2.7	4.3	3.1	3.7	0.32	1.5	3.8	4.4	3.0	3.8	4.3	2.5	2.9	0.24
Ru	4.3	2.1	3.3	2.1	5.3	1.5	3.8	2.4	4.3	3.0	4.4	0.75	1.9	4.5	4.7	3.9	3.8	5.4	2.7	3.5	0.13
Pt	7.6	5.4	5.1	5.4	3.7	4.4	6.6	5.4	8.5	5.8	9.4	3.6	8.0	11.5	7.7	15.7	10.2	15.1	3.5	10.4	0.86
Pd	6.5	3.9	5.8	4.2	0.6	3.3	3.9	5.2	6.6	5.0	7.8	2.8	4.9	50.2	7.4	4.0	7.5	10.9	1.2	17.4	2.1

[a] Concentrations are in ppb. The concentrations of Himalayan samples are reported by *Guillot et al.* [2001].
[b] Cumu indicates cumulates.

field for abyssal peridotites, defined by 10th and 90th percentile values of 126 samples compiled by *Niu* [2004] (Figure 5b).

[26] Most samples from Cuba plot in the field of abyssal peridotites on an Al/Si versus Mg/Si diagram (Figure 5b), but two samples, Cu51 and Cu63, show low Al/Si and plot in an area similar to that from the Himalayas and Mariana forearc serpentinites. As mentioned, these two samples differ in spinel composition and texture from the rest of the Cuban samples, and resemble Himalayan samples (Figure 5b). The difference in bulk rock compositions, and the texture and composition of spinel suggests that the two serpentinite samples are different from the rest of the Cuban samples; they may be similar to forearc-mantle serpentinites from the Himalayas.

[27] The ratios of Mg/Si and Al/Si appear to provide definite parameters indicating a primary nature of the protoliths of the peridotites, but not all major elements are immobile. The CaO is highly mobile, and its depletion is noted in all samples from the Alps and most samples from Cuba (Figure 6). The data suggest that alteration of clinopyroxene is accompanied by dissolution of Ca.

[28] The Mg# values (atomic ratios of $Mg/[Mg + Fe^{2+}]$ or $Mg/[Mg + \Sigma Fe]$) in bulk rocks) are commonly used to show the degree of depletion after partial melting; however, we do not use these values since it is not possible to determine the concentrations of Fe^{2+} in spinel-containing rocks. Furthermore, the Mg# appears not as sensitive as Al/Si ratios as a parameter for the degrees of partial melting, since most serpentinite samples have a similar Mg#, ~0.90, using total Fe content.

5.2. Minor and Trace Elements

[29] The compositions of serpentinites indicate the enrichment of fluid-mobile elements (Figure 6). To quantify the degrees of enrichment, we selected Ce as a reference, although Ce is still mobile in hydrothermal fluids (Figure 6). Strictly speaking, therefore, Ce is not a suitable reference, but it is the most abundant REE and its concentrations are available from many other samples in literature. Furthermore, Ce is considered to have a similar incompatibility as Pb during partial melting in mantle peridotites [e.g., *Hofmann et al.*, 1986; *Noll et al.*, 1996]. Therefore Ce was used as a reference to compare the degrees of mobility of other fluid-mobile elements (Figures 7a and 7b). The ratios of
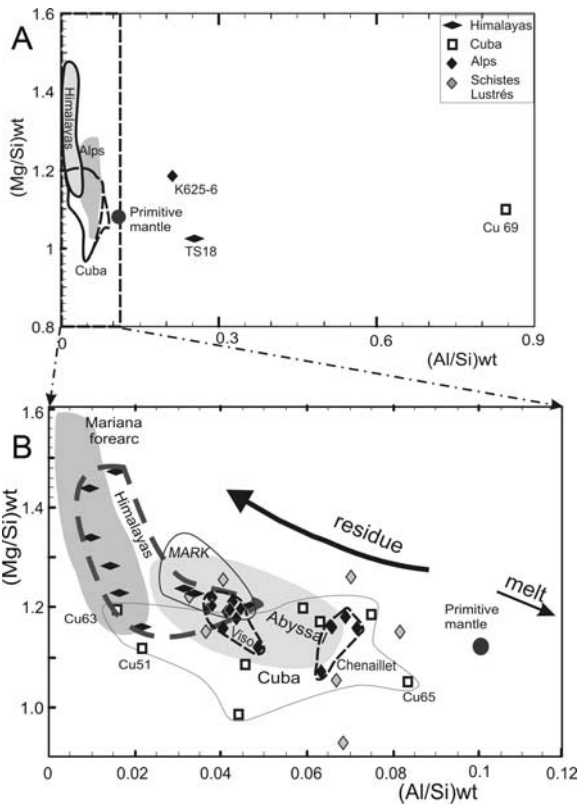
Figure 5. Weight ratios of Mg/Si versus Al/Si of serpentinite samples. The large solid circle with the primitive mantle value is from *McDonough and Sun* [1995]. Mariana forearc peridotites are from *Ishii et al.* [1992], *Yamamoto et al.* [1992], and *Parkinson and Pearce* [1998]. The field of hydrated peridotites, mostly harzburgites, from the MARK section, mid-Atlantic ridge (light solid line), is from *Burgath et al.* [1997] and *Casey* [1997]. Serpentinites from the MARK region are mostly refractory harzburgites and not totally enclosed within the abyssal peridotite field (light shaded area) that is defined by 10th and 90th percentile values of 126 abyssal peridotite samples compiled by *Niu* [2004]. Data from Alps include those obtained by *Chalot-Prat et al.* [2003], shown in diamonds, Chenaillet and Monviso (solid diamonds), and Schistes Lustrés (grey diamonds). The compositional variation expected during partial melting is shown with arrows. Residues have higher Mg/Si and lower Al/Si, whereas melt has a lower Mg/Si and higher Al/Si. Symbols are the same in Figure 4 for Himalayan samples (flat diamonds) and Cuban samples (squares). Note the large compositional variation for Cuban samples, because they originated from peridotites in a mantle wedge and also abyssal peridotites.

Pb/Ce for our serpentinites show that Pb is highly enriched in comparison to anhydrous abyssal peridotites; also, the enrichment is greatest in Himalayan samples (Figure 7a). Cuban and Al-

pine samples show the enrichment of soluble chalcophile elements, but not as great as Himalayan samples (Figure 7a). Two samples from the deformation zone in Cuba, which were noted for their different spinel textures and low Al/Si compared to other Cuban samples, show evidence for a high enrichment of chalcophile elements, including Pb, in comparison to the other Cuban samples (Figure 7a).

[30] Chalcophile elements have an affinity with S and are commonly concentrated in sulphide minerals in crustal rocks. Our earlier X-ray absorption study [*Hattori et al.*, 2005] indicates that As in Himalayan serpentinites is mostly As^{5+}, and that As is not hosted by sulphides. Instead, As is hosted by oxides and antigorite in the samples. The low concentrations of S and the lack of positive correlations between the concentrations of these chalcophile elements and S also support this interpretation.
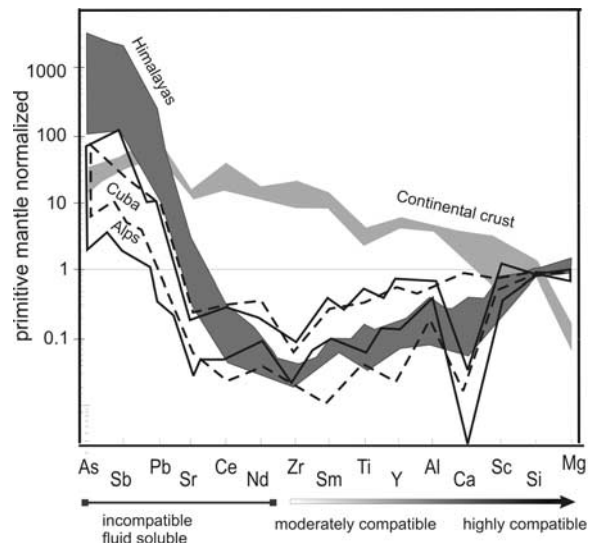

Figure 6. Normalized concentrations of fluid-mobile and fluid-immobile elements in serpentinites from Himalaya compared to samples of continental crust and arc magmas at volcanic fronts. Fluid-mobile elements refer to those with high solubilities in aqueous fluids. Most fluid-mobile elements have similar compatibility with light rare earth elements during partial melting but are on the left side of the x axis to show their enrichment and to clarify the diagram. Fluid-immobile elements are listed in order of compatibility with mantle minerals during partial melting. Serpentinites and continental crust are normalized to primitive mantle [*McDonough and Sun*, 1995]. The values of bulk continental crust are from *Taylor and McLennan* [1995]. Note that the enrichment patterns of serpentinites are different from those of the crustal rocks. Therefore simple physical contamination by crustal rocks does not explain the enrichment of fluid-mobile elements.
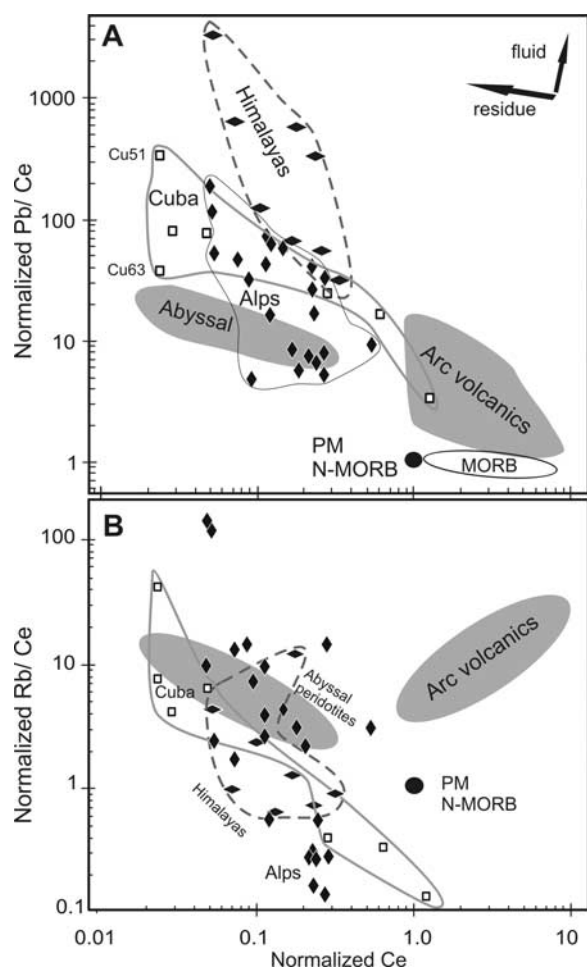
Figure 7. Primitive mantle normalized Ce versus Pb/Ce (Figure 7a) and Rb/Ce ratios (Figure 7b) of serpentinites. The field for abyssal peridotites (light shaded area) is based on 10th and 90th percentile values of 126 samples by *Niu* [2004]. Data from Alps include those determined by *Chalot-Prat et al.* [2003] and are shown as diamonds. The primitive mantle value of Pb is from *McDonough and Sun* [1995]. Rubidium content of the primitive mantle used is 0.4975 ppm, 0.025 times the Sr content. To eliminate the melt-solid fractionation of elements, arc volcanic rock values are normalized to N-MORB values of 0.489 ppm Pb, 7.5 ppm Ce, and 0.56 ppm Rb. The volcanic rocks are those at volcanic fronts, listed by *Hattori and Guillot* [2003]. Rubidium was used to represent alkalis because the concentrations of Rb were precisely determined using isotopic dilution.

[31] We examined the degrees of the enrichment of alkalis using Rb/Ce ratios, using Rb to represent alkalis instead of the more abundant K because the concentrations of Rb were precisely determined using the isotope dilution technique.

[32] Alkalis are highly soluble in water at relatively low temperatures, but their enrichment in serpentinites is not as apparent as Pb. The primitive mantle-normalized ratios of Rb/Ce are comparable to or lower than those of abyssal peridotites, indicating that there is essentially no enrichment of Rb during the hydration of peridotites. High Rb/Ce ratios are observed in several serpentinites from the Alps, especially those from Schistes Lustrés accretionary prism that is dominated by metasedimentary rocks [e.g., *Agard et al.*, 2001]. Because sediments contain high Rb and low REE, high observed ratios of Rb/Ce are most likely explained by the incorporation of aqueous fluids from sediments.

5.3. Platinum Group Elements

[33] All mantle peridotite samples contain high Ir-type PGE (Os, Ir and Ru), comparable to primitive mantle values (Figure 8 and Table 2d), confirming that they are mantle residues of partial melting because refractory Ir-type PGE are low in partial melts [e.g., *Righter et al.*, 2004; *Brenan et al.*, 2005]. Samples identified as ultramafic cumulates, on the basis of high Al/Si ratios in bulk-rock compositions (Figure 5a), contain low Ir-type PGE compared to the primitive mantle values (Figure 8). For example, ultramafic cumulate samples TS18 and Cu69 (Figure 5a) plot outside the field for mantle peridotites; rather, they are similar to ultramafic cumulates from the base of Talkeetna arc, Alaska, and the base of the Kohistan arc (Figure 8).

[34] Among the PGE, Cuban and Alpine samples show a significant variation in Pd contents with comparable concentrations of Ir. For example, sample K624-10 from Lago Superiore in Monviso contains low Pd, 0.59 ppb, which is much lower than other samples from the Alps (3.3 to 7.2 ppb Pd), even lower than the primitive mantle value. The variation of Pd concentration is most likely explained by its relatively high mobility in aqueous fluids [e.g., *Hattori and Cameron*, 2004; *Hinchey and Hattori*, 2005].

5.4. Strontium Isotope Compositions

[35] All serpentinite samples discussed here have elevated $^{87}Sr/^{86}Sr$ values compared to those of mantle rocks. The Himalayan samples in particular show very high $^{87}Sr/^{86}Sr$, ~0.72. Such high $^{87}Sr/^{86}Sr$ ratios are indicative of ancient crustal material and are consistent with low εNd, as low as −15 in the samples, reported by *Guillot et al.* [2001]. Cuban and Alpine samples vary from 0.703 to ~0.710. The low values are similar to
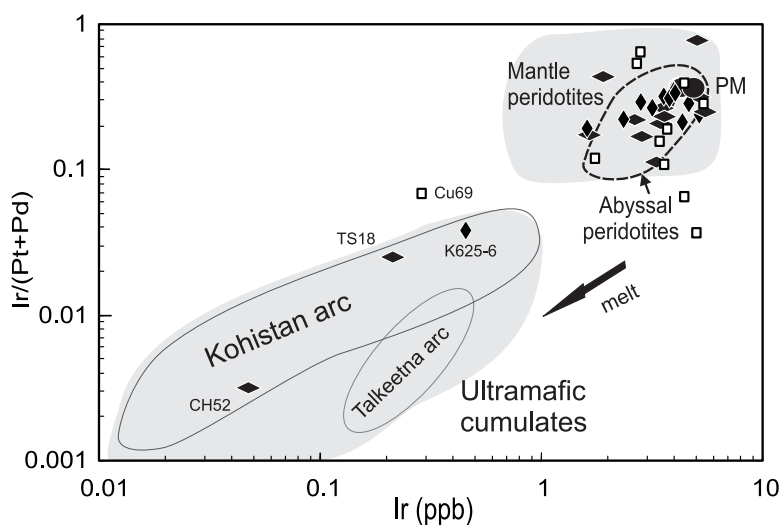
Figure 8. Iridium and Ir/(Pt + Pd) weight ratios of bulk rocks. Primitive mantle value is shown with a large solid circle, labeled PM. The field for mantle peridotites includes abyssal peridotites [*Snow and Schmidt*, 1998; *Rehkämper et al.*, 1999], Horoman, Japan [*Rehkämper et al.*, 1999], Ronda and Beni Bousera [*Garuti et al.*, 1996; *Gueddari et al.*, 1996], and Zabargad, Red Sea [*Schmidt et al.*, 2000]. The fields for ultramafic cumulates include data from the Jijal ultramafic complex at the base of the Kohistan arc, northern Pakistan [*Hattori and Shirahase*, 1997], and Talkeetna arc [*Hattori and Hart*, 1997]. The symbols are the same as in Figure 5. Iridium is a refractory Ir-type PGE, whereas Pt and Pd are preferentially incorporated in partial melt. Therefore the ratios of Ir/Pt + Pd are expected to be low in partial melt.

the upper mantle value of 0.7027 [e.g., *Allègre et al.*, 1983], whereas the high values are similar to $^{87}Sr/^{86}Sr$ of present-day marine Sr, ∼0.709 [*Faure*, 2005] (Figure 9). Considering that marine $^{87}Sr/^{86}Sr$ values were lower in the Tertiary than the present value, these elevated $^{87}Sr/^{86}Sr$ values suggest a contribution of Sr from sedimentary rocks. This is not surprising since sedimentary rocks dominate in the Schistes Lustrés, and are significant, ∼20 vol%, at Monviso. These sedimentary rocks have a high $^{87}Sr/^{86}Sr$ signature [e.g., *Amato et al.*, 1999]. Our Sr isotopic data are similar to those for three serpentinite samples obtained from Schistes Lustrés and Monviso by *Chalot-Prat et al.* [2003] (Figure 9).

5.5. Sulphur Concentrations and Isotope Compositions of Serpentinites

[36] Himalayan samples have low concentrations of S, all less than 51 ppm S. Most samples contain S below the Kiba-method detection limit of 4 ppm S. Therefore only a limited number of samples yielded S isotopic compositions; these values have a relatively narrow spread, ranging from −6.5 to + 4.3‰ (Table 3). *Alt and Shanks* [2006] found high concentrations, up to 3,588 ppm, of sulphate S in Mariana forearc serpentinites, but we did not find any sulphate S in our samples. A high concentration

of S is present in one sample (TS 18C) in the Himalayan serpentinites, collected at the base of Nidar arc ophiolite complex (Figure 1a). It contains 744 ppm S and is enriched in ^{34}S, +12.6‰ (Table 3).

[37] Most Alpine and Cuban samples contain S below 4 ppm, except for two cumulate samples (K625-5 and K625-6) from the Alps containing high S, up to 2400 ppm S (Table 3). All Cuban serpentinites yielded low S contents, <5 ppm. The data are surprising considering that they originated from abyssal peridotites, and that high concentrations of sulphide S (up to 1 wt%) are reported for serpentinites in the MARK area of the mid-Atlantic ridge [e.g., *Alt and Shanks*, 2003]. Isotopic compositions of sulphide S that were measurable in our samples are overall enriched in ^{34}S, from +11 to +17‰ (Table 3), which is consistent with the contribution of ^{34}S-rich marine sulphate S. This is distinct from all but one of the Himalayan samples.

6. Discussion

6.1. Protoliths of Serpentinites

[38] Major-element concentrations of serpentinites indicate that the Himalayan samples originated from highly refractory peridotites. Both bulk-rock compositions and chromian spinel data for the
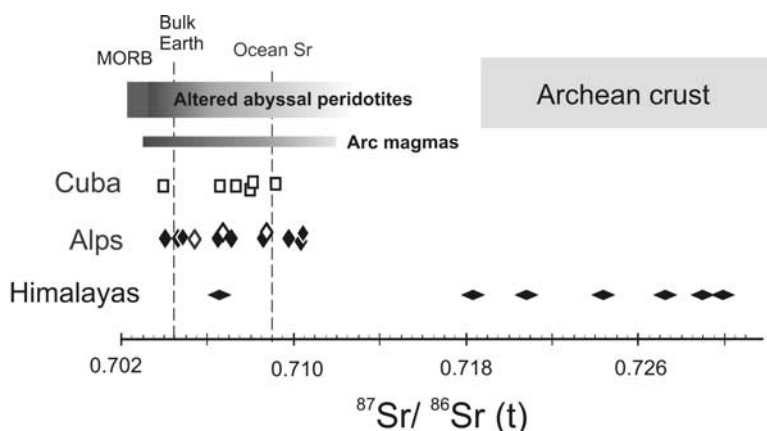
Figure 9. Strontium isotope compositions of serpentinites. Symbols for Cuba (open squares) and Himalaya (flat diamonds) are the same as in Figure 5. Alps data include three serpentinite samples (open tall diamonds) from *Chalot-Prat et al.* [2003]. Shaded area shows the values for mid-oceanic ridge basalts (MORB), abyssal peridotites altered by seawater [*Kimball and Gerlach*, 1986; *Snow et al.*, 1994], and arc magmas [*Heath et al.*, 1998; *Faure*, 2005].

Himalayan serpentinites are similar to those of Mariana forearc serpentinites. The Himalayan serpentinite samples are closely associated with the Tso Morari UHP unit [*Guillot et al.*, 2001], a metamorphic product of continental margin sediments. There are no oceanic rocks in the vicinity of the area. Therefore these serpentinites originated from the base of the forearc-mantle wedge overlying the subducted Indian continent underlying the margin of Eurasia.

[39] Most Cuban and Alpine samples have variably less refractory geochemical signatures, with significant concentrations of Al and Ca in bulk-rock compositions compared to the Himalayan samples (Figure 5b). These serpentinites are comparable in bulk-rock composition to abyssal peridotites (Figure 5), and such an origin of the serpentinites is supported by their occurrences. In Cuba and the Alps, serpentinites are voluminous and are associated with omphacitic eclogites, which are metamorphic products of oceanic basalts and gabbros [e.g., *Pognante and Kienast*, 1987; *Schneider et al.*, 2004].

[40] Two Cuban samples (Cu51 and Cu63) from the deformation zone between the northern margin of the UHP Zaza zone and the base of arc igneous rocks show lower Al/Si in bulk-rock compositions than the majority of Cuban serpentinites (Figure 5b). Low Al/Si ratios are similar to the Himalayan and Mariana forearc serpentinites (Figure 5b). In addition, chromite is still present in cores of spinel grains and rimmed by ferritchromite and magnetite in these two Cuban samples. The texture of spinel grains is similar to that of spinel in Himalayan serpentinites.

These two samples are interpreted to be mantle-wedge peridotites, but Cr# in spinel grains are distinctly low compared to the Himalayan samples (Figure 4). Moderate values of Cr# are consistent with the relatively low Mg/Si ratios for bulk-rock compositions compared to high ratios of the Himalayan and Mariana forearc serpentinites (Figure 5b), suggesting that the Cuban mantle wedge was not as refractory as that in the more mature subduction systems of the Himalayas and Mariana. In Cuba, the southward subduction of the Proto-Caribbean oceanic plate just started in the late Cretaceous, shortly before exhumation of the serpentinites.

[41] An abyssal peridotite origin of all Alpine samples and most Cuban samples agrees with their association with omphacitic eclogites, which were originally oceanic basalts and gabbros before high-pressure metamorphism in subduction zones [e.g., *Pognante and Kienast*, 1987; *Schneider et al.*, 2004]. Furthermore, this interpretation is also supported by the nature of subducted oceanic plates in Cuba and the Alps, i.e., produced at very slow spreading ridges [e.g., *Lagabrielle and Cannat*, 1990; *Pindell et al.*, 1988]. Oceanic plates produced at slow- to ultraslow-spreading ridges, such as the Atlantic Ocean plate, commonly contain thin and discontinuous basaltic crust [e.g., *Gràcia et al.*, 1977; *Dick et al.*, 2003] and exhibit abundant exposure of mantle peridotites on the seafloor [e.g., *Cannat*, 1993; *Cannat et al.*, 1997; *Lagabrielle et al.*, 1998; *Mével*, 2003].

[42] The oceanic origin of our samples from the Alps and Cuba is further supported by micro-

Table 3. Sulphur Contents and Isotope Compositions of Bulk Rock Samples

	Location	S Content, ppm	$\delta^{34}S_{CD}$, ‰
	Himalayas		
CH98a	Zildat fault	34	+4.3
CH98b	Zildat fault	48	+2.8
CH146	Zildat fault	6	
CH187	Zildat fault	30	−0.49
CH422	Zildat fault	8	
CH423	Zildat fault	51	−6.7
CH433	Zildat fault	<5	
CH35a	Nidar arc	<5	
TS18c	Nidar arc	740	+12.3
	Alps		
S623-1	Monviso	347	+17.4
K624-2	Monviso	<5	
K624-10	Monviso	<5	
S625-5	cumulate, Monviso	1630	+11.9
K625-6	cumulate, Monviso	2410	+11.7
	Cuba		
Cu24	Escambray	<5	
Cu51	south of Zaza zone	<5	
Cu54	Zaza zone	<5	
Cu55	Zaza zone	<5	

Raman spectral data that show low-temperature serpentine minerals as early phases and high-temperature antigorite as a late phase [*Auzende et al.*, 2002, 2006] (Figure 3). Serpentinization in abyssal peridotites mostly takes place at relatively low temperatures, on or near the seafloor, and is followed by antigorite formation during subduction of the oceanic plate.

[43] Alpine serpentinites possess district-scale compositional variations (Figure 5b). The serpentinites in the Chenaillet massif are least refractory compared to most abyssal peridotites and serpentinites in the Monviso massif, suggesting that the two massifs represent two different areas. The Schistes Lustrés serpentinites show a large compositional variation, ranging between those of the Monviso and Chenaillet samples. This variation supports the origin of Schistes Lustrés as being a metasedimentary accretionary prism containing different slices of oceanic lithosphere [*Agard et al.*, 2001]. The least refractory nature of peridotites in the Chenaillet massif agrees with the composition data of basaltic rocks from the massif. *Chalot-Prat et al.* [2003] showed that the basalts have an affinity with "enriched mid-oceanic ridge basalts

(E-MORB)". Considering the geological events in the area, oceanic rocks in the early formed Chenaillet massif were likely produced at an immature oceanic ridge near continents. The geochemical signature of E-MORB from the igneous rocks is explained by interaction with continental lithosphere. On the other hand, the oceanic rocks now in the Monviso massif were produced at a fully developed ridge, with little influence from distant continents; they are therefore more refractory than the Chenaillet samples.

[44] The above discussion emphasizes that major-element ratios of Mg/Si and Al/Si did not change during the hydration and metamorphism of peridotites, and also that the ratios reflect those of anhydrous peridotites. The hydration of peridotites in the mantle wedge was presumably continuous at low to high temperatures, >300°C, and high pressures. The serpentinization of abyssal peridotites may occur at high temperature, associated with ocean-ridge hydrothermal activity. Furthermore, serpentinites in oceanic lithosphere were heated again when they were subducted. Although Al, Si and Mg are relatively immobile, Si is known to migrate in aqueous fluids at temperatures as low as 400°C [*Allen and Seyfried*, 2003]. Thus such loss of Si may cause higher Mg/Si and Al/Si ratios in serpentinites than anhydrous peridotites. However, we discount this possible mobility of Si as the cause for the observed variation of Mg/Si and Al/Si in our samples. First, the data do not show a positive slope expected from the loss or addition of Si (Figure 5b). Secondly, the major-element compositions of serpentinites of partially and totally hydrated peridotites in each district are very similar to one another. For example, samples Cu55 and Cu56 are close, <1 km from each, in the Zaza zone in Cuba; Cu55 retains unaltered pyroxenes and olivine with 6.1 wt% loss of ignition (LOI), whereas sample Cu56 is fully hydrated with 13.7 wt% LOI. The ratios of Al/Si and Mg/Si for the two samples are very similar, ~0.06 for Al/Si and ~1.19 for Mg/Si. Similarly, all samples from Monviso have a very small variation in Mg/Si versus Al/Si ratios, even though they have different degrees of hydration, ranging from 3 to 13 wt% H_2O (Figure 5b). Thirdly, peridotites in the MARK region of the Mid-Atlantic ridge show a wide range in LOI, from 4 to 13 wt% [*Casey*, 1997], but the weight ratios of Al/Si and Mg/Si are similar (Figure 5b). This generalization also applies to peridotites from Mariana forearc serpentinites [e.g., *Ishii et al.*, 1992; *Yamamoto et al.*, 1992; *Parkinson and Pearce*, 1998; *Savov et al.*, 2005].

Variably serpentinized peridotites show a similarly low Al/Si ratio. Therefore the ratios of Mg/Si and Al/Si likely represent those of the primary peridotites. The concentrations of Si, Al and Mg are readily available and these data provide useful criteria to identify serpentinite sources.

[45] This proposed interpretation, no significant change in Mg/Si and Al/Si during hydration to form serpentinites, does not mean that the concentrations of all major elements remained constant. Among the major elements, Ca is clearly mobile (Figure 6). For example, the content of CaO in fully serpentinitized Cu56 is 0.14 wt%, compared to 3.12 wt% in partially serpentinized sample Cu55, both of which were collected within a short distance, less than 100 m of each other. The depletion of CaO is most prominent in Alpine serpentinites (Figure 6). A depletion of CaO has been noted in hydrated abyssal peridotites by previous workers, such as *King et al.* [2003], who reported progressively lower CaO in more hydrated peridotites in the accretionary prism of the Franciscan Complex. This evidence suggests that CaO is removed by seawater during hydration of abyssal peridotites on or near the seafloor or ridge hydrothermal systems. The depletion of Ca from ultramafic rocks during the interaction with seawater is further supported by experimental data. *Allen and Seyfried* [2003] noted in their hydrothermal experiments that Ca is quickly leached by saline waters from clinopyroxene-bearing ultramafic rocks. The high mobility of Ca is also supported by elevated concentrations of Ca in seawater that has reacted with abyssal peridotites [e.g., *Kelley et al.*, 2001]. Other supporting evidence is the occurrence of abundant calcite pillars near submarine hydrothermal vents in regions dominated by ultramafic rocks, such as Lost City [e.g., *Kelley et al.*, 2001; *Früh-Green et al.*, 2003]. Therefore both field observations and experimental data suggest that clinopyroxene and amphiboles are not stable during serpentinization, and readily release Ca during their hydration. This high mobility of Ca is consistent with the very rare retention of clinopyroxene grains in our serpentinites.

6.2. Source of Water for the Hydration of Peridotites

[46] The sources of water for hydration are considered on the basis of the protoliths of the serpentinites. For forearc-mantle peridotites, it appears that they were hydrated by the water released from subducted slabs. For abyssal peridotites, it is likely

that seawater contributed to the hydration. The sources of water can be further evaluated using isotope data.

[47] Strontium isotope compositions of serpentinites agree with the forearc-mantle origin of Himalayan samples, and an abyssal-peridotite origin of most Alpine and Cuban samples. In the Himalayas, the northern margin of the Indian continent was subducted below the southern margin of Eurasia after collision between the two continents at the time of the Paleocene-Eocene boundary, at ~55 Ma [e.g., *Leech et al.*, 2005]. There were shallow-water sediments on the margin of the Indian continent including evaporites, sandstones, and mudstones [e.g., *Steck et al.*, 1993]. Evaporites formed in such a semi-closed sedimentary basin commonly have higher $^{87}Sr/^{86}Sr$ than oceanic Sr because of the influx of riverine Sr from the surrounding continents. Furthermore, the clastic components of these sediments were derived from Precambrian granitic gneisses on the northern margin of the Indian continent, which have high $^{87}Sr/^{86}Sr$ (>0.72 [*Whittington et al.*, 2000]). During subduction, water and fluid-mobile elements were released from these immature sediments and moved upward to the base of the mantle wedge. They were introduced and incorporated into the overlying serpentinites.

[48] We consider that the high concentrations of fluid-mobile elements in the Himalayan samples are explained by their uptake from the subducting slab during hydration of peridotites. It may be argued instead that crustal water may have participated in the hydration of peridotites during their exhumation. We discount this possibility. Once peridotites are hydrated, serpentinites would not incorporate any more aqueous fluids, since unlike smectite minerals, serpentine minerals do not have interlayer sites to accommodate water molecules. Furthermore, serpentine minerals in the Himalayan serpentinites are still mostly antigorite with minor late veins of crysotile. The preservation of antigorite suggests that its composition was likely retained. In addition, numerical modeling suggests that the buoyancy and low viscosity of serpentinites are critical for the exhumation of dense eclogites [e.g., *Schwartz et al.*, 2001; *Gerya et al.*, 2002]. To achieve this buoyancy and low viscosity, the peridotites had to be hydrated before initiation of exhumation of the accompanying eclogites at a depth ~100 km.

[49] For the Alpine and most Cuban samples, the hydration of peridotites most likely was caused by

Table 4. Strontium Isotope Compositions of Serpentinites[a]

	Location[b]	$^{87}Sr/^{86}Sr$ Present	Rb, ppm	Sr, ppm	$^{87}Sr/^{86}Sr$ (t)[c]
		Himalayas			
CH98a	Zildat	0.72998 ± 3	0.08	23	0.72997
CH98b	Zildat	0.72435 ± 4	0.07	13	0.72434
CH146	Zildat	0.70653 ± 3	0.033	30	0.70653
CH187	Zildat	0.72080 ± 5	0.11	7	0.72076
CH422	Zildat	0.72896 ± 10	0.10	9	0.72893
CH423	Zildat	0.72716 ± 2	0.11	7	0.72712
CH433	Zildat	0.71831 ± 2	0.14	55	0.71831
		Cuba			
Cu24	Escam	0.70810 ± 3	0.052	0.73	0.70776
Cu54	Zaza	0.70669 ± 3	0.10	4.11	0.70657
Cu55	Zaza	0.70802 ± 2	0.50	1.35	0.70622
Cu62	Zaza	0.70375 ± 4	0.22	11.0	0.70365
Cu69	Escam	0.70733 ± 1	0.28	5.12	0.70707
		Alps			
K621-4	Chena	0.70716 ± 6	0.24	7.65	0.70698
K622-3	Lustrés	0.71047 ± 2	0.32	1.91	0.70954
K622-3b	Lustrés	0.71033 ± 5	0.36	5.70	0.70998
S623-1	Viso	0.70478 ± 1	0.28	3.64	0.70435
K624-3	Viso	0.70854 ± 8	0.063	0.445	0.70774
K624-7	Viso	0.70977 ± 2	0.036	0.19	0.70869
S625-5	Viso	0.70397 ± 1	0.11	230	0.70397
K625-6	Viso	0.70463 ± 2	0.028	10.8	0.70462

[a] Longitudes and latitudes of sample locations are in Tables 2a–2d. Cu24, only antigorite, from the Escambray massif, associated with eclogites; Cu54, predominantly antigorite with minor chrysotile and talc, from the Zaza zone, embedded with eclogites; Cu55, partially serpentinized lherzolite with the primary olivine (Fo = 90) and pyroxene grains, associated with amphibolite facies metabasalts in the Zaza zone; serpentine minerals are mostly chrysotile with veinlets of a mixture of chrysotile + lizardite, later cut by antigorite (Figure 3), cumulate with high Si and low Mg (plotted outside Figure 5a) in Zaza zone, associated with eclogites; Cu69, cumulate (Figure 5a), mélange zone of Escambray massif, greenschist facies nappe; K621-4, base of Chenaillet ophiolite; K622-3, Queyras Schistes Lustrés; K622-3B, fissile samples adjacent to K622-3; S623-1, Monviso; K624-3, Monviso; K624-7, Monviso; K 625-6 and S625-6.

[b] Escam, Escambray, Cuba; Lustrés, Shistes Lustrés, Alps; Viso, Monviso, Alps; Zaza, Zaza zone, Cuba; Zildat, Zildat fault, Himalayas.

[c] Initial $^{87}Sr/^{86}Sr$ values are calculated at 60 Ma for Himalayan samples, 120 Ma for Cuban samples [*Pindell et al.*, 2005], and 140 Ma for the Alpine samples [*Lemoine et al.*, 1987]. Small errors in ages do not have a significant effect in the calculated initial $^{87}Sr/^{86}Sr$ because of low Rb/Sr ratios.

seawater, considering that their bulk-rock compositions are very similar to those of abyssal peridotites, and that their associated omphacitic eclogites were originally oceanic basalts and gabbros. This conclusion is supported by ^{34}S-enriched sulphide S and $^{87}Sr/^{86}Sr$. Although S contents of the Alpine and Cuban samples are low compared to serpentinites in the MARK region [*Alt and Shanks*, 2003], the $\delta^{34}S$ values for sulphide S, >15‰, in the serpentinites from the Alps are high. Signifi-

cant enrichment of ^{34}S in S is consistent with the contribution of marine S, ~+20‰. Other supporting evidence is provided by high $^{87}Sr/^{86}Sr$ values for serpentinites compared to the upper mantle value (Figure 9); most values are similar to the present-day marine Sr value. Considering that there was a lower $^{87}Sr/^{86}Sr$ ratio of marine Sr in the Paleocene-Eocene than the present-day [*McArthur et al.*, 2001], a high $^{87}Sr/^{86}Sr$ ratio suggests a contribution of Sr from abundant sediments, which likely accumulate on a slow-spreading oceanic plate. Abyssal peridotites and oceanic basalts are known to acquire Sr in solution during alteration with seawater, as evidenced by the low contents of Sr in anhydrous peridotites [e.g., *Kimball and Gerlach*, 1986; *Snow et al.*, 1994].

[50] Sample K621-4 collected from the base of Chenaillet massif has a rather low $^{87}Sr/^{86}Sr$ ratio (0.707 at 140 Ma) compared to the values of ~0.710 for serpentinite samples from Schistes Lustrés and Monviso (Table 4). Our data are consistent with the finding of *Chalot-Prat et al.* [2003], who analyzed one serpentinite sample each from Chenaillet, Schistes Lustrés and Monviso, and also found rather low $^{87}Sr/^{86}Sr$ (140 Ma) of 0.7054 from a serpentinite sample collected at the base of the Chenaillet massif. The Chenaillet massif does not contain abundant sediments, as does the Shistes Lustrés or the Monviso massif. This lack of sediments overlying ultramafic rocks may partially explain the rather low Sr isotope ratios. In addition, the Chenaillet massif is considered to have formed near continents [e.g., *Agard et al.*, 2001] and the abyssal peridotites were not exposed to seawater for as long a time as the others.

6.3. Transfer of Fluid-Mobile Elements From Slabs to Mantle Wedges

6.3.1. Forearc-Mantle Serpentinites

[51] The serpentinite samples are variably enriched in soluble chalcophile elements, including As, Sb, and Pb [*Hattori and Guillot*, 2003] (Figure 6). Our earlier X-ray absorption study indicates that As occurs in the +5 state in Himalayan serpentinites, suggesting that As^{5+} was transferred by aqueous fluids from a slab under oxidized condition at shallow depths, <25 km [*Hattori et al.*, 2005].

[52] The Himalayan samples show the greatest enrichment in these chalcophile elements compared to the Alpine and Cuban samples (Figures 6 and 7a). This difference between the Himalayan samples

and the others is explained by the different modes of hydration among the three locations. The fore-arc-mantle peridotites in the Himalayas were hydrated by water released from a slab, with aqueous fluids ascending to the overlying mantle wedge, causing hydration of forearc-mantle peridotites. During fluid ascent, the concentrations in solution continually increase because water is continuously consumed by the hydration of peridotites, concentrating the soluble ions in solution. Highly concentrated elements are eventually incorporated in serpentinites, after all the water in the aqueous fluid is consumed. This concentration mechanism is probably the reason why serpentinites that originate from mantle wedges are enriched in fluid-mobile elements.

[53] As mentioned above, two Cuban samples (Cu51, Cu63) from the deformation zone adjacent to arc rocks most likely originated from the mantle wedge overlying the subducted oceanic plate, on the basis of low Al/Si ratios (Figure 5b), relatively high Cr# of chromite (Figure 3), and the texture of the chromite. It is interesting to note that these two samples contain high concentrations of Pb of all the Cuban samples.

[54] The hydration process of forearc-mantle peridotites suggests that the concentrations of fluid-mobile elements in forearc-mantle serpentinites may vary depending on the subducted material. For example, Mariana forearc serpentinites and Himalayan serpentinites show similar Mg/Si and Al/Si ratios (Figure 5b), but the concentrations of fluid-mobile elements differ greatly. The Mariana forearc serpentinites are underlain by subducted Pacific Ocean lithosphere, whereas the Himalayan serpentinites were underlain by shallow-water sediments on the margin of the Indian continent. Himalayan samples contain high As, up to 275 ppm [*Hattori et al.*, 2005], whereas Mariana forearc serpentinites contain less than 2.5 ppm As, with an average of 0.48 ppm [*Savov et al.*, 2005]. High As in the Himalayan serpentinites is explained by the high As contents that are common in shallow-water sediments [e.g., *Togashi et al.*, 2000; *Smedley and Kinniburgh*, 2002]. In addition, granitic clasts in the shallow-water sediments were most likely high in As content and other soluble chalcophile elements [*Smedley and Kinniburgh*, 2002].

[55] Serpentinites in forearc mantle may display a compositional gradient with distance from the subducted slabs. Large quantities of water pass through serpentinites in direct contact with the subducting plates and the serpentinites may not

be highly enriched in many elements discharged from slabs. On the other hand, partially hydrated peridotites may be highly enriched in fluid-mobile elements because water may have been totally consumed by hydration reactions, leaving all initially dissolved elements to remain in the rocks during hydration. Some elements may not be fixed immediately during hydration; for example, serpentinites in the Himalayas are low in S because evaporites containing sulphate were subducted, which kept the base of the mantle wedge oxidized, as indicated by the occurrence of As^{+5} in those serpentinites [*Hattori et al.*, 2005]. The SO_4^{2-} released from the slab was eventually fixed as sulphides in the overlying peridotites because the fO_2 of the aqueous fluids decreased during ascent. The Fe^{2+} released from hydrating olivine and pyroxenes also reduces the fO_2 of fluids during serpentinization [e.g., *Sleep et al.*, 2004].

[56] The variables that affect the abundance of fluid-mobile elements in forearc serpentinites, discussed above, make it difficult to evaluate the global average composition of forearc serpentinites. Furthermore, a volume of serpentinites would be required to evaluate the net amounts of such element recycling in subduction zones, but the distribution of forearc serpentinites is not yet fully characterized from geophysical data [e.g., *Kamiya and Kobayashi*, 2000; *Bostock et al.*, 2002; *Brocher et al.*, 2003; *Blakely et al.*, 2005; *Ramachandran et al.*, 2005]. Numerical simulations show that the size and distribution of serpentinites may vary greatly along the subduction zones depending on many parameters, such as subduction angle and the nature of subducting plate [e.g., *Gerya et al.*, 2002].

6.3.2. Hydrated Abyssal Peridotites

[57] The mode of hydration for serpentinites in the Alps and Cuba is distinctly different from that in the Himalayas. All Alpine and most Cuban serpentinite samples originated from abyssal peridotites and were most likely hydrated by seawater. These serpentinites were also enriched in fluid-mobile elements by seawater that circulated through sediments, basalts and peridotites, but these elements could not be highly enriched in seawater simply circulating in fractures.

[58] High sulphide S contents are commonly recorded in serpentinites formed in oceanic environments; high sulphide S contents are explained by the reduction of marine SO_4^{2-} to S^{2-} during serpentinization [e.g., *Alt and Shanks*, 2003]. How-

ever, only two Alpine samples contain significant concentrations of sulphide S in our serpentinite samples; the otherwise low concentrations of sulphide S in our samples from the Alps and Cuba suggest that sulphide may have been removed during subduction, either by decomposition or dissolution. We discount the former possibility because sulphide minerals, mostly pyrrhotite and pentlandite, are stable at temperatures above 600°C. One possible explanation is the relatively high solubility of sulphur in aqueous fluids. During subduction of oceanic lithosphere, sediments lose much of their H_2O at shallow depths, <30 km [*Rüpke et al.*, 2004], whereas underlying altered basalts release H_2O gradually during the entire path of metamorphism. Serpentine minerals remain, but sulphides may dissolve in hot aqueous fluids released from sediments and altered basalts, to be transferred to the overlying mantle wedges.

6.4. Transfer of Fluid-Mobile Elements From Slabs to Arc Magmas

[59] Arc magmas are characterized by elevated concentrations of large-ion lithophile elements and fluid-mobile elements [*Ryan et al.*, 1995; *Noll et al.*, 1996]. The commonly held view suggests that the eclogitization of slabs releases aqueous fluids to the overlying mantle wedges; the water then causes partial melting, forming arc magmas [e.g., *Peacock*, 1993]. *Rüpke et al.* [2004] demonstrated evidence for the continuous release of fluid from subducting slabs, with over 40 vol% water in sediments released in the very early stages of subduction, at depths shallower than 30 km. This conclusion is supported by the occurrence of As^{+5} in Himalayan serpentinites, because oxidized As^{+5} is most commonly released from sediments at shallow levels, <25 km [*Hattori et al.*, 2005]. To explain the apparent contradiction between the lack of volcanism in forearc regions and the continuous release of fluids from slabs, *Hattori and Guillot* [2003] suggested that the aqueous fluids released from slabs is incorporated in a layer of serpentinites at the base of mantle wedges; thus formation of serpentinite layers keeps the interiors of the wedges dry. The serpentinites at the base of wedges are subsequently dragged down to greater depths by mantle corner flow; the eventual decomposition of serpentinites at a depth of ~100 km releases water to the interior of mantle wedges, leading to partial melting and the generation of arc magmatism at volcanic fronts.

[60] The proposed interpretation for arc magmatism is based on our study of Himalayan forearc-mantle serpentinites; this is also applicable to oceanic subduction zones, where voluminous abyssal serpentinites are present in the subducting plates. Because the stability of serpentine minerals is pressure-sensitive, serpentinites both overlying and underlying the plates would decompose to orthopyroxene + olivine + water at a depth of ~100 km [*Wünder et al.*, 2001]. Elements that cannot be accommodated in orthopyroxene and olivine would be partitioned into the fluid phase and ascend to the interior of the mantle wedge. These fluid-mobile elements are then incorporated into arc magmas during partial melting. Therefore the abundance of fluid-mobile elements in arc magmas at volcanic fronts reflects the compositions of subducted slabs, because forearc-mantle serpentinites are the primary transient reservoir for these elements in the mantle.

6.5. Differentiation of Fluid-Mobile Elements

[61] Alkalis are highly soluble in water, but their concentrations are not significant in our serpentinite samples. The low concentrations of alkalis in forearc-mantle serpentinites may be attributed to their retention in subducting slabs. In slabs, alkalis reside in phengite and amphiboles in sediments and altered igneous rocks [e.g., *Bach et al.*, 2003]. Amphibole minerals break down to form clinopyroxene during eclogitization of slabs at the depth of ~80 km [e.g., *Peacock*, 1993], but sodium and other alkalis released from amphiboles are retained in clinopyroxene and phengite. Phengite has a wide stability field and is stable in subducting slabs until a depth of ~300 km [e.g., *Domanik and Holloway*, 2000]. Sodium in clinopyroxene remains in slabs at even deeper levels.

[62] Alkalis are not high in volcanic-front magmas, and their concentrations increase in arc magmas with increasing distance from trenches [e.g., *Gill*, 1981; *Ryan et al.*, 1995]; this is consistent with the low concentrations measured in our forearc serpentinites, because dehydration of serpentinites at ~100 km likely triggers partial melting for volcanic front magmas [*Hattori and Guillot*, 2003].

7. Summary

[63] Serpentinites associated with HP and UHP rocks have three possible origins: ultramafic cumulates, abyssal peridotites, and mantle peridotites

from overlying wedges. This study shows that the ratios of Mg/Si and Al/Si provide clear parameters to identify their origins. Himalayan samples are mostly derived from a refractory forearc-mantle wedge with low Al/Si, similar to the Mariana forearc serpentinites. They were hydrated by water released from the subducted margin of the Indian continent and therefore have high concentrations of fluid-mobile elements and high $^{87}Sr/^{86}Sr$ ratios.

[64] Serpentinites from forearc-mantle wedges show a strong enrichment of fluid-mobile elements. These elements and radiogenic isotope signatures are transferred to greater depths in the mantle as serpentinites are dragged down in the mantle by mantle corner flow. Eventual breakdown of serpentinite minerals releases water and fluid-mobile elements, contributing to mantle metasomatism in the mantle wedge and arc magmas. Considering the mode of serpentinization, the abundances of fluid-mobile elements in forearc mantle serpentinites varies greatly depending on the subducted material.

[65] Serpentinites from oceanic subduction zones, such as in Cuba and the Alps, are associated with high-pressure omphacitic rocks. The association suggest that these serpentinites originated mostly from abyssal peridotites of oceanic plates produced at slow spreading ridges. Alpine serpentinites show a nappe-by-nappe major-element compositional variation, reflecting different domains of abyssal peridotites. Serpentinites from the Chenaillet massif represent fertile peridotites, those from the Monviso refractory peridotites and Schistes Lustrés contain a variety of peridotites.

[66] The abyssal peridotites were hydrated by seawater to form lizardite and minor chrysotile and talc on or near the ocean floor at low temperatures. They were subsequently transformed to antigorite during subduction. The enrichment of soluble elements is not as great as that in the forearc mantle peridotites because hydration took place under a high water/rock ratio environment.

[67] Cuban serpentinites that occur along a major shear deformation are not abyssal peridotites, but originated from a forearc-mantle wedge and show many similarities with the Himalayan forearc mantle serpentinites. This evidence suggests that minor forearc-mantle peridotites can also occur in an oceanic subduction environment.

[68] A lack of alkali enrichment is noted in all serpentinites in this study. Such data suggest that alkalis are retained in sediments and subducted slabs until a depth of ~300 km, where phengite may break down. This wide pressure range of the stability of alkali-bearing phases is consistent with the relatively low contents of alkalis in volcanic front magmas and their high concentrations in magmas associated with back-arc volcanism.

Acknowledgments

References

Agard, P., L. Jolivet, and B. Goffé (2001), Tectonometamorphic evolution of the Schistes Lustrés complex: Implications for the exhumation of HP and UP rocks in the Western Alps, *Bull. Soc. Geol. Fr.*, *172*, 617–636.

Agard, P., P. Monié, L. Jolivet, and B. Goffé (2002), Exhumation of the Schistes Lustrés complex: In situ laser probe $^{40}Ar/^{39}Ar$ constraints and implications for the Western Alps, *J. Metamorph. Geol.*, *20*, 599–618.

Allègre, C. J., S. R. Hart, and J. F. Minster (1983), Chemical structure and evolution of the mantle and continents determined by inversion of Nd and Sr isotopic data, II. Numerical experiments and discussion, *Earth Planet. Sci. Lett.*, *66*, 191–213.

Allen, D. E., and W. E. Seyfried Jr. (2003), Compositional controls on vent fluids from ultramafic-hosted hydrothermal systems at mid-ocean ridges: An experimental study at 400°C, 500 bars, *Geochim. Cosmochim. Acta*, *67*, 1531–1542.

Alt, J. C., and W. C. Shanks III (2003), Serpentinization of abyssal peridotites from the MARK area, Mid-Atlantic Ridge: Sulphur geochemistry and reaction modeling, *Geochim. Cosmochim. Acta*, *67*, 641–653.

Alt, J. C., and W. C. Shanks III (2006), Stable isotope compositions of serpentinite seamounts in the Mariana forearc: Serpentinization processes, fluid sources and sulfur metasomatism, *Earth Planet. Sci. Lett.*, *242*, 272–285.

Amato, J. M., C. M. Johnson, L. P. Baumgartner, and B. L. Beard (1999), Rapid exhumation of the Zermatt-Saas ophiolite deduced from high-precision Sm-Nd and Rb-Sr geochronology, *Earth Planet. Sci. Lett.*, *171*, 238–425.

Auzende, A., B. Devouard, S. Guillot, I. Daniel, A. Baronnet, and J. M. Lardeaux (2002), Serpentinites from central Cuba: Petrology and HRTEM study, *Eur. J. Mineral.*, *14*, 905–914.

Auzende, A. L., S. Guillot, B. Devouard, and A. Baronnet (2006), Serpentinites in Alpine convergent setting: Effects of metamorphic grade and deformation on microstructures, *Eur. J. Mineral.*, *18*, 21–33.

Bach, W., N. R. Banerjee, H. J. B. Dick, and E. T. Baker (2002), Discovery of ancient and active hydrothermal systems along the ultra-slow spreading Southwest Indian Ridge 10°–16°E, *Geochem. Geophys. Geosyst.*, *3*(7), 1044, doi:10.1029/2001GC000279.

Bach, W., B. Peucker-Ehrenbrink, S. R. Hart, and J. S. Blusztajn (2003), Geochemistry of hydrothermally altered oceanic crust: DSDP/ODP Hole 504B – Implications for seawater-crust exchange budgets and Sr- and Pb-isotopic evolution of the mantle, *Geochem. Geophys. Geosyst.*, *4*(3), 8904, doi:10.1029/2002GC000419.

Barnes, S. J., and P. L. Roeder (2001), The range of spinel compositions in terrestrial mafic and ultramafic rocks, *J. Petrol.*, *42*, 2279–2302.

Blake, M. C., D. E. Moore, and A. S. Jayko (1995), The role of the serpentinite mélange in the unroofing of UHPM rocks: An example from Western Alps of Italy, in *Ultrahigh Pressure Metamorphism*, edited by R. G. Coleman and X. Wang, pp. 182–205, Cambridge Univ. Press., New York.

Blakely, R. J., T. M. Brocher, and R. E. Wells (2005), Subduction zone magnetic anomalies and implications for hydrated forearc mantle, *Geology*, *3*, 445–448.

Bostock, M. G., R. D. Hyndman, S. Rondenay, and S. M. Peacock (2002), An inverted continental Moho and serpentinization of the forearc mantle, *Nature*, *417*, 536–538.

Brenan, J. M., W. F. McDonough, and R. Ash (2005), An experimental study of the solubility and partitioning of iridium, osmium and gold between olivine and silicate melt, *Earth Planet. Sci. Lett.*, *237*, 855–872.

Brocher, T. M., T. Parsons, A. M. Trehu, C. M. Snelson, and M. A. Fisher (2003), Seismic evidence for widespread serpentinized forearc upper mantle along the Cascadia margin, *Geology*, *31*, 267–270.

Burgath, K. P., V. Marching, and K. Mussallam (1997), Data report: Mineralogical, structural and chemical variability of mantle sections from Holes 920B and 920D, *Proc. Ocean Drill. Program Sci. Results*, *153*, 505–520.

Burke, K. (1988), Tectonic evolution of the Caribbean, *Annu. Rev. Earth Planet. Sci.*, *16*, 201–230.

Caby, R. (1996), Low-angle extrusion of high-pressure rocks and the balance between outward and inward displacements of middle Penninin units in the Western Alps, *Eclogae Geol. Helv.*, *89*, 229–267.

Cannat, M. (1993), Emplacement of mantle rocks in the sea-floor at mid-ocean ridges, *J. Geophys. Res.*, *98*, 4163–4172.

Cannat, M., Y. Lagabrielle, H. Bougault, J. Casey, N. de Coutures, L. Dmitriev, and Y. Fouquet (1997), Ultramafic and gabbroic exposures at the Mid-Atlantic Ridge: Geological mapping in the 15°N region, *Tectonophysics*, *279*, 193–213.

Casey, J. F. (1997), Comparison of major- and trace-element geochemistry of abyssal peridotites and mafic plutonic rocks with basalt from the Mark region of the Mid-Atlantic Ridge, *Proc. Ocean Drilling Program Sci. Results*, *153*, 181–241.

Chalot-Prat, F., J. Ganne, and A. Lombard (2003), No significant element transfer from the oceanic plate to the mantle wedge during subduction and exhumation of the Tethys lithosphere (Western Alps), *Lithos*, *69*, 69–103.

de Sigoyer, J., S. Guillot, and P. Dick (2004), Exhumation of the ultrahigh-pressure Tso Morari unit in eastern Ladakh (NW Himalaya): A case study, *Tectonics*, *23*, TC3003, doi:10.1029/2002TC001492.

Dick, H. J. B., and T. Bullen (1984), Chromian spinel as a petrogenetic indicator in abyssal and alpine-type peridotites and spatially associated lavas, *Contrib. Mineral. Petrol.*, *86*, 54–76.

Dick, H. J. B., J. Lin, and H. Schouten (2003), An ultraslow-spreading class of ocean ridge, *Nature*, *426*, 405–412.

Dobson, D. P., P. G. Meredith, and S. A. Boon (2002), Simulation of subduction zone seismicity by dehydration of serpentine, *Science*, *298*, 1407–1410.

Domanik, K. J., and J. R. Holloway (2000), Experimental synthesis and phase relations of phengiti muscovite from 6.5 to 11 GPa in a calcareous metapelite from the Dabie Mountains, China, *Lithos*, *52*, 51–77.

Evans, B. W. (1977), Metamorphism of Alpine peridotite and serpentinite, *Annu. Rev. Earth Planet. Sci.*, *5*, 397–447.

Faure, G. (2005), *Origin of Igneous Rocks: The Isotopic Evidence*, 494 pp., Springer, New York.

Früh-Green, G. L., D. S. Kelley, S. M. Bernasconi, J. A. Karson, K. A. Ludwig, D. A. Butterfield, C. Boschi, and G. Proskurowski (2003), 30,000 years of hydrothermal activity at the Lost City Vent Field, *Science*, *301*, 495–498.

Garuti, G., M. Oddone, and J. Torres-Ruiz (1996), Platinum-group element distribution in subcontinental mantle: Evidence from the Ivrea zone (Italy), and the Betic-Rifean cordillera (Spain and Morocco), *Can. J. Earth Sci.*, *34*, 444–463.

Gerya, T. V., B. Stöckhert, and A. L. Perchuk (2002), Exhumation of high-pressure metamorphic rocks in a subduction channel: A numerical simulation, *Tectonics*, *21*(6), 1056, doi:10.1029/2002TC001406.

Gill, J. (1981), *Orogenic Andesites and Plate Tectonics*, 390 pp., Springer, New York.

Gràcia, E., D. Bideau, R. Hekinian, Y. Lagabrielle, and L. M. Parson (1977), Along-axis magmatic oscillations and exposure of ultramafic rocks in a second-order segment of the Mid-Atlantic Ridge (33°43′N to 34°07′N), *Geology*, *25*, 1059–1062.

Gueddari, K., M. Piboule, and J. Amosse (1996), Differentiation of platinum-group elements (PGEs), and of gold during partial melting of peridotites in the lherzolitic massif of the Betico-Rifean range (Ronda and Beni Bousera), *Chem. Geol.*, *134*, 181–197.

Guillot, S., K. H. Hattori, and J. de Sigoyer (2000), Mantle wedge serpentinization and exhumation of eclogites: Insights from eastern Ladakh, NW Himalaya, *Geology*, *28*, 199–202.

Guillot, S., K. Hattori, J. de Sigoyer, T. Nagler, and A. L. Auzende (2001), Evidence of hydration of the mantle wedge and its role in the exhumation of eclogites, *Earth Planet. Sci. Lett.*, *193*, 115–127.

Hacker, B. R. (1996), Eclogite formation and the rheology, buoyancy, seismicity, and H_2O content of oceanic crust, in *Subduction: Top to Bottom*, *Geophys. Monogr. Ser.*, vol. 96, edited by G. E. Bebout et al., pp. 337–346, AGU, Washington, D. C.

Hart, S. R., and C. Brooks (1977), The geochemistry and evolution of early Precambrian mantle, *Contrib. Mineral. Petrol.*, *61*, 109–128.

Hattori, K. H., and E. M. Cameron (2004), Utilizing the high mobility of palladium in exploration for platinum group element mineralization: Evidence from the Lac des Iles area, Canada, *Econ. Geol.*, *99*, 157–171.

Hattori, K. H., and S. Guillot (2003), Volcanic fronts form as a consequence of serpentinite dehydration in the forearc mantle wedge, *Geology*, *31*, 525–528.

Hattori, K., and S. R. Hart (1997), PGE and Os isotopic signatures for ultramafic rocks from the base of the Talkeetna island arc, Alaska, *Eos Trans. AGU*, *78*(17), 339.

Hattori, K., and T. Shirahase (1997), Platinum group elements and osmium isotope signatures of Kohistan Island arc sequence, Himalaya-Korakaram area, *Eos Trans. AGU*, *78*(46), Fall Meet. Suppl., F829.

Hattori, K. H., L. J. Cabri, B. Johanson, and M. L. Zientek (2004), Origin of placer laurite from Borneo: Se and As contents, and S isotopic compositions, *Min. Mag.*, *68*, 353–368.

Hattori, K., Y. Takahashi, S. Guillot, and B. Johanson (2005), Occurrence of arsenic (V), in forearc mantle serpentinites: X-ray absorption spectroscopy study, *Geochim. Cosmochim. Acta.*, *69*, 5585–5596.

Heath, E., R. Macdonald, H. Belkin, C. Hawkesworth, and A. Sigurdsson (1998), Magmagenesis at Soufriere volcano, St. Vincent, Lesser Antilles Arc, *J. Petrol.*, *39*, 1721–1764.

Hinchey, J. G., and K. H. Hattori (2005), Magmatic mineralization and hydrothermal enrichment of the High Grade Zone at the Lac des Iles palladium mine, northern Ontario, Canada, *Miner. Deposita*, *40*, 3–23.

Hofmann, A. K., P. Jochum, M. Seufert, and W. M. White (1986), Nb and Pb in oceanic basalts: New constraints on mantle evolution, *Earth Planet. Sci. Lett.*, *79*, 33–45.

Horen, H., M. Zamora, and G. Dubuisson (1996), Seismic wave velocities and anisotropy in serpentinized peridotites from Xigaze ophiolite: Abundance of serpentine in slow spreading ridge, *Geophys. Res. Lett.*, *23*, 9–12.

Hutson, F., P. Mann, and P. Renne (1998), $^{40}Ar/^{39}Ar$ dating of single muscovite grains in Jurassic siliciclastic rocks (San Cayetano Formation): Constraints on the paleoposition of western Cuba, *Geology*, *26*, 83–86.

Ishii, T., P. T. Robinson, H. Maekawa, and R. Fiske (1992), Petrological studies of peridotites from diapiric serpentinites seamounts in the Izu-Ogasawara-Mariana forearc, Leg 125, *Proc. Ocean Drill. Program Sci. Results*, *125*, 445–463.

Kamiya, S., and Y. Kobayashi (2000), Seismological evidence for the existence of serpentinized wedge mantle, *Geophys. Res. Lett.*, *27*, 819–822.

Kelley, D. S., et al. (2001), An off-axis hydrothermal vent field near the Mid-Atlantic Ridge at 30°N, *Nature*, *412*, 145–148.

Kimball, K. L., and D. C. Gerlach (1986), Sr isotopic constraints on hydrothermal alteration of ultramafic rocks in two oceanic fracture zones from the South Atlantic Ocean, *Earth Planet. Sci. Lett.*, *78*, 177–188.

King, R. L., M. J. Kohn, and J. M. Eiler (2003), Constraints on the petrologic structure of the subduction zone slab-mantle interface for Franciscan Complex exotic ultramafic blocks, *Geol. Soc. Am. Bull.*, *115*, 1097–1109.

Lagabrielle, Y., and M. Cannat (1990), Alpine Jurassic ophiolites resemble the modern central Atlantic basement, *Geology*, *18*, 319–322.

Lagabrielle, Y., D. Bideau, M. Cannat, J. A. Karson, and C. Mével (1998), Ultramafic-mafic plutoic rock suites exposed along the Mid-Atlantic Ridge (10°N–30°N): Symmetrical-asymmetrical distribution and implications for seafloor spreading processes, in *Faulting and Magmatism at Mid-Ocean Ridges*, *Geophys. Monogr. Ser.*, vol. 106, edited by W. R. Buck et al., pp. 153–176, AGU, Washington, D. C.

Lardeaux, J. M., S. Schwartz, P. Tricart, A. Paul, S. Guillot, N. Béthoux, and F. Masson (2006), A crustal-scale cross-section of the south-western Alps combining geophysical and geological imagery, *Terra Nova*, *18*, 412–422.

Leech, M. L., S. Singh, A. K. Jain, S. L. Klemperer, and R. M. Manickavasagam (2005), The onset of India-Asia continental collision: Early, steep subduction required by the timing of UHP metamorphism in the western Himalaya, *Earth Planet. Sci. Lett.*, *234*, 83–97.

Lemoine, M., P. Tricart, and G. Boillot (1987), Ultramafic and gabbroic ocean floor of the Ligurian Tethys (Alps, Corsica, Apennines): In search of a genetic model, *Geology*, *15*, 622–625.

Lombardo, B., D. Rubatto, and D. Castelli (2002), Ion microprobe U-Pb dating of zircon from a Monviso metaplagiogranite: Implications for the evolution of the Piedmont-Liguri Tethys in the western Alps, *Ofioliti*, *27*, 109–117.

McArthur, J. M., R. J. Howarth, and T. R. Bailey (2001), Strontium isotope stratigraphy: LOWESS version 3: Best fit to the marine Sr-isotope curve for 0–509 Ma and accompanying look-up tale for deriving numerical age, *J. Geol.*, *109*, 155–170.

McDonough, W., and S. S. Sun (1995), The composition of the Earth, *Chem. Geol.*, *120*, 223–253.

Mével, C. (2003), Serpentinization of abyssal peridotites at mid-ocean ridges, *C. R. Geosci.*, *335*, 825–852.

Millán, G. (1993), Evolucion de la estructura del macizo de Escambray, sur de Cuba central, *Cienc. Tierra Espacio*, *21–22*, 26–45.

Millán, G. (1997), Geología del macizo detamórfico del Escambray, in *Estudios Sobre Geología de Cuba*, edited by G. F. Furrazola Bermúdez and K. E. Núñez Cambra, pp. 271–288, Cent. Nac. de Inf. Geol., Havana.

Niu, Y. (2004), Bulk-rock major and trace element compositions of abyssal peridotites: Implications for mantle melting, melt extraction and post-melting processes beneath mid-ocean ridges, *J. Petrol.*, *45*, 2423–2458.

Noll, P. D., Jr., H. E. Newsom, W. P. Leeman, and J. G. Ryan (1996), The role of hydrothermal fluids in the production of subduction zone magmas: Evidence from siderophile and chalcophile trace elements and boron, *Geochim. Cosmochim. Acta*, *60*, 587–611.

O'Brien, P., N. Zotov, R. Law, A. M. Kahn, and M. Q. Jan (2001), Coesite in Himalayan eclogite and implication for models of India-Asia collision, *Geology*, *29*, 435–438.

Parkinson, I. J., and J. A. Pearce (1998), Peridotites from the Izu-Bonin-Mariana forearc (ODP Leg 125), Evidence for mantle melting and melt-mantle interaction in a supra-subduction zone setting, *J. Petrol.*, *39*, 1577–1618.

Peacock, S. M. (1993), Metamorphism, dehydration, and importance of the blueschist- eclogite transition in subducting oceanic crust, *Geol. Soc. Am. Bull.*, *105*, 684–694.

Pindell, J. L., S. C. Cande, W. C. Pitman III, D. B. Rowley, J. F. Dewey, J. L. LaBrecque, and W. F. Haxby (1988), A plate-kinematic framework for models of Caribbean evolution, *Tectonophysics*, *155*, 121–138.

Pindell, J., L. Kennan, W. V. Maresch, K. P. Stanek, G. Draper, and R. Higgs (2005), Plate-kinematics and crustal dynamics of circum-Caribbean arc-continent interactions: Tectonic controls on basin development in Proto-Caribbean margins, *Spec. Pap. Geol. Soc. Am.*, *394*, 7–52.

Piotrowska, K. (1993), Interrelationship of the terranes in western and central Cuba, *Tectonophysics*, *220*, 273–282.

Pognante, U., and J. R. Kienast (1987), Blueschist and eclogite transformations in Fe-Ti gabbros: A case from the Western Alps ophiolites, *J. Petrol.*, *28*, 271–292.

Ramachandran, K., S. E. Dosso, G. D. Spence, R. D. Hyndman, and T. M. Brocher (2005), Forearc structure beneath southwestern British Columbia: A three-dimensional tomographic velocity model, *J. Geophys. Res.*, *110*, B02303, doi:10.1029/2004JB003258.

Ravizza, G., and D. Pyle (1997), PGEs and Os isotopic analyses of single sample aliquots with NiS fire assay preconcentration, *Chem. Geol.*, *141*, 251–268.

Rehkämper, M., A. N. Halliday, J. Alt, J. G. Fitton, J. Zipfel, and E. Takazawa (1999), Non-chondritic platinum-group element ratios in oceanic mantle lithosphere: Petrogenetic signature of melt percolation?, *Earth Planet. Sci. Lett.*, *172*, 65–81.

Righter, K., A. J. Campbell, M. Humayun, and R. L. Hervig (2004), Partitioning of Ru, Rh, Pd, Re, Ir and Au between Cr-bearing spinel, olivine, pyroxene and silicate melts, *Geochim. Cosmochim. Acta*, *68*, 867–880.

Rüpke, L. H., J. P. Morgan, M. Hort, and J. A. D. Connolly (2004), Serpentine and the subduction zone water cycle, *Earth Planet. Sci. Lett.*, *223*, 17–34.

Ryan, J. G., J. Morris, F. Tera, W. P. Leeman, and A. Tsvetkov (1995), Cross-arc geochemical variations in the Kurile arc as a function of slab depth, *Science*, *270*, 625–627.

Sasaki, A., T. Arikawa, and R. E. Folinsbee (1979), Kiba reagent method of sulphur extraction applied to isotope work, *Bull. Geol. Surv. Jpn.*, *30*, 241–245.

Savov, I. P., J. G. Ryan, M. D'Antonio, K. Kelley, and P. Mattie (2005), Geochemistry of serpentinized peridotites from the Mariana Forearc Conical Seamount, ODP Leg 125: Implications for the elemental recycling at subduction zones, *Geochem. Geophys. Geosyst.*, *6*, Q04J15, doi:10.1029/2004GC000777.

Scambelluri, M., G. B. Piccardo, P. Philippot, A. Robbiano, and L. Negretti (1997), High salinity fluid inclusions formed from recycled seawater in deeply subducted alpine serpentinites, *Earth Planet. Science Lett.*, *148*, 485–499.

Schmidt, G., H. Palme, K.-L. Kratz, and G. Kurat (2000), Are highly siderophile elements (PGE, Re and Au), fractionated in the upper mantle of the Earth? New results on peridotites from Zabargad, *Chem. Geol.*, *163*, 167–188.

Schneider, J., D. Bosch, P. Monie, S. Guillot, A. Garcia-Casco, J. M. Lardeaux, R. L. Torres-Roldan, and G. M. Trujillo (2004), Origin and evolution of the Escambray Massif (central Cuba): An example of HP/LT rocks exhumed during intraoceanic subduction, *J. Metamorph. Geol.*, *22*, 227–247.

Schwartz, S., P. Allemand, and S. Guillot (2001), Numerical model of effect of serpentinites on the exhumation of eclogitic rocks: Insights from the Monviso ophiolitic massif (Western Alps), *Tectonophysics*, *342*, 193–206.

Sleep, N. H., A. Meibom, Th. Fridriksson, R. G. Voleman, and D. K. Bird (2004), H_2-rich fluids from serpentinization: Geochemical and biotic implications, *Proc. Natl. Acad. Sci. U. S. A.*, *101*, 12,818–12,823.

Smedley, P. L., and D. G. Kinniburgh (2002), A review of the source, behaviour and distribution of arsenic in natural waters, *Appl. Geochem.*, *17*, 517–568.

Snow, J. E., and G. Schmidt (1998), Constraints on earth accretion deduced from noble metals in the oceanic mantle, *Nature*, *391*, 166–169.

Snow, J. E., S. R. Hart, and H. J. B. Dick (1994), Nd and Sr isotope evidence linking mid-ocean-ridge basalts and abyssal peridotites, *Nature*, *371*, 57–60.

Soyer, W., and M. Unworth (2006), Deep electrical structure of the northern Cascadia (British Columbia, Canada), subduction zone: Implications for the distribution of fluids, *Geology*, *34*, 53–56.

Stanek, K. P., W. V. Maresch, F. Grafe, Ch. Grevel, and A. Baumann (2006), Structure, tectonics and metamorphic development of the Sancti Spiritus Dome (Eastern Escambray massif, Central Cuba), *Geol. Acta*, *4*, 151–170.

Steck, A., L. Spring, J. C. Vannay, H. Masson, H. Bucher, E. Stutz, R. Marchant, and J. C. Tieche (1993), Geological transect across the northwestern Himalaya in eastern Ladakh and Lahul: A model for the continental collision of India and Asia, *Eclogae Geol. Helv.*, *86*, 219–263.

Taylor, S. R., and S. M. McLennan (1995), The geochemical evolution of the continental crust, *Rev. Geophys.*, *33*, 241–265.

Togashi, S., N. Imai, Y. Okuyama-Kusunose, T. Tanaka, T. Okai, T. Koma, and Y. Murata (2000), Young upper crustal chemical composition of the orogenic Japan Arc, *Geochem. Geophys. Geosyst.*, *1*(11), doi:10.1029/2000GC000083.

Whittington, A., N. B. W. Harris, M. W. Ayres, and G. Foster (2000), Tracing the origins of the western Himalaya: An isotopic comparison of the Nanga Parbat massif and Zanskar Himalaya, in *Tectonics of the Nanga Parbat Syntaxis and the Western Himalaya*, edited by M. A. Khan et al., *Geol. Soc. Spec. Publ.*, *170*, 201–218.

Wünder, B., R. Wirth, and M. Gottschalk (2001), Antigorite: Pressure and temperature dependence of polysomatism and water content, *Eur. J. Mineral.*, *13*, 485–495.

Yamamoto, K., N. Matsutani, N. Nakamura, and T. Ishii (1992), REE characteristics of mafic rocks from a forearc seamount in the Izu-Ogasawara region, western Pacific, *Geochem. J.*, *26*, 411–423.